ACTIVE MINIMIZATION OF ENERGY DENSITY IN THREE-DIMENSIONAL ENCLOSURES

Summary of Research

Dec. 1993 - Dec. 1995

Principal Investigator

Scott D. Sommerfeldt
Dept. of Physics & Astronomy
Brigham Young University
Provo, UT 84602

and

Applied Research Laboratory
The Pennsylvania State University
P.O. Box 30
State College, PA 16804

NASA Grant No. NAG-1-1557

June 18, 1996

ACTIVE MINIMIZATION OF ENERGY DENSITY IN THREE-DIMENSIONAL ENCLOSURES

Summary of Research
Dec. 1993 - Dec. 1995

Scott D. Sommerfeldt
(Principal Investigator)

Dept. of Physics & Astronomy
Brigham Young University
Provo, UT 84602

and

Applied Research Laboratory
The Pennsylvania State University
P.O. Box 30
State College, PA 16804

NASA Grant No. NAG-1-1557

June 18, 1996

Table of Contents

List of Figures

List of Tables

ACTIVE MINIMIZATION OF ENERGY DENSITY IN THREE-DIMENSIONAL ENCLOSURES

I. Introduction

In many applications involving noise in enclosures, the desired control objective is to globally minimize the noise in the enclosure, or to at least minimize the noise over some extended region. Such applications include interior noise in aircraft, automobiles, and rooms. For a regularly-shaped enclosure, such as a rectangular enclosure, it is possible to analytically determine the optimal solution for a control source(s) which will minimize the total potential energy in the enclosure, as has been demonstrated by Nelson *et al.*[1] The effect of minimizing the potential energy is to generally attenuate the overall sound pressure level throughout the enclosure. However, the total potential energy is a quantity that is not available in practice, since it requires spatially integrating the entire acoustic field.

The objective of this study was to further investigate and develop a novel approach for actively controlling the sound field in enclosures that is based on the acoustic energy density. Typically the acoustic field in an enclosure has been controlled by minimizing the sum of the squared pressures from several microphones distributed throughout the enclosure. The approach investigated in this study involved minimizing the acoustic energy density at the sensor locations, rather than the squared pressure. Research previous to this study[2] in a simple one-dimensional enclosure showed that improved global attenuation of the acoustic field is often obtained by minimizing the energy density, rather than the pressure. The current study built on the previous research by extending the method of controlling the acoustic energy density to three-dimensional enclosures. The study was intended to help establish if improved control can still be expected in a more general enclosure.

The study was designed to be both analytical/numerical and experimental in nature. The numerical analysis provided valuable insights in guiding the experimental efforts. As part of the experimental effort, a three-dimensional "energy density sensor" was developed and implemented to test the control approach. The purpose of this summary report is to overview the results obtained in the course of the study.

2. Summary

A study has been completed to examine the effectiveness of actively minimizing the energy density in enclosures, as a means of achieving greater global control of the interior field. The approach has been tested both numerically and experimentally in three-dimensional enclosures. It should be noted that the focus of the study was on sensing issues, and not on actuator issues. As such, little or no attempt was made in the research to optimize the number and locations of the actuators used. The most significant results of the study can be summarized as follows:

i) It was demonstrated that it is possible to fabricate an inexpensive three-dimensional "energy density sensor" that could be used both for active control implementation, as well as for a general investigation of the acoustic field. This was significant, since at the onset of the study, the only energy density sensor that had been developed was a one-dimensional sensor that used two relatively expensive phase-matched B&K microphones. The low cost of the current three-dimensional sensor makes potential practical implementations feasible.

ii) The numerical and experimental results confirmed the hypothesis that for a given number of sensors, controlling the energy density generally provided global control of the field that was as good as, and in most cases better than, the control achieved using pressure as the acoustic quantity to be minimized. It should be noted that an energy density sensor consists of multiple transducers (currently six microphones), so that this statement does not reflect a comparison of transducers, but of error sensors.

iii) It was found that for multiple error sensors (i.e. N sensors), the control achieved using energy density control was generally comparable to the control achieved using approximately 6N pressure microphones, in the traditional manner. Thus, if one makes the comparison based only on the number of transducers used, the differences were generally not significant. However, the controller architecture is simpler with N energy density sensors than 6N pressure sensors.

iv) It was also found that the global control achieved using energy density sensors was considerably less dependent on sensor location than when using pressure sensors. This result has important practical implications, since it suggests that the energy density sensors can generally be placed wherever it is practical, without seriously affecting the control of the field that will be achieved.

3. Background and Program Objectives

The current research study reported here was precipitated by a prior study that was begun in 1990 as a M.S. thesis project at The Pennsylvania State University[2]. In this prior study, the question was posed as to whether improved global attenuation could be achieved in an enclosed acoustic field by minimizing the energy density, rather than the pressure. The decision to investigate this approach was based on the observation that practical implementations for global control were beginning to use large numbers of error sensors (i.e. ~ 50) to control interior acoustic fields. As a result, it was desired to investigate possible approaches that would potentially reduce the number of error sensors required. This prior study was restricted to one-dimensional fields to simplify the investigation. The result of that study was that it was found that significant improvement in the global control could be achieved by controlling the energy density. However, it was also recognized that the one-dimensional field was somewhat lacking in generality, and thus it was desired to extend the research to three-dimensional fields. As well, for the prior study, an energy density sensor was developed that was suitable for one-dimensional fields, but was not suitable for three-dimensional fields. In addition, the previous energy density sensor was rather expensive, which potentially made practical implementation somewhat prohibitive. Nonetheless, the prior study was very successful in terms of developing the control approach for minimizing energy density[3], as well as in demonstrating the basic proof of concept.

Following the prior study, it was desired to extend the concepts developed to three-dimensional fields, which is the basis of this current study. In this phase of the study there were several restrictions and objectives. The study was restricted to a study of low modal-density acoustic fields, which corresponds to the lower frequency range. It is important to keep this restriction in mind when analyzing the results, since different control mechanisms can be expected for high modal-density fields vs. low modal-density fields. An additional restriction in this phase of the research was that the number of actuators was restricted to be less than or equal to the number of error sensors. It is possible to implement more actuators than sensors, but that requires modifications to the control system to remove the indeterminacy that normally results. It is envisioned that future research will remove this limitation. Finally, since the focus of the research was on sensing issues, little or no attempt was made to optimize either the number or the locations of the control actuators. Rather, the problem was simply posed as: Given the actuator configuration, what is the best control that can be achieved by minimizing either the energy density or the pressure?

In view of the previous restrictions, there were a number of objectives that the study was designed to accomplish. It was desired to develop a three-dimensional energy density sensor that was practical for implementation. The sensor would need to be able to accurately determine the energy density quantities of interest, and would also need to be relatively inexpensive to be practical for many implementations. It was also desired to gain a greater understanding of three-dimensional acoustic fields and how the control system interacts with the field to achieve either global or local attenuation of the field. Finally, a principle objective of the research was to compare the control that could be achieved using energy density sensors with the control achieved using pressure sensors. This comparison was made in one of two ways. One comparison was with equal numbers of sensor

sites, and the other comparison was with equal numbers of transducers. The two comparisons result from the fact that energy density sensors require multiple transducers for implementation.

4. Results of the Study

4.1 Theoretical Development

For an active control application, the acoustic field in a rectangular enclosure can be thought of as consisting of two components: the pressure due to the primary source(s), and the pressure due to the secondary source(s). In general, the control that can be achieved in the enclosure will depend on the location of the sources, the location of the error sensors used, and the choice of the performance function chosen for the control system. As mentioned previously, the purpose of this project was to compare the control that can be achieved using several different performance functions, for a given arbitrary source and sensor configuration. As a result, for the results shown below, there has been no attempt to optimize any of the source or sensor locations. The focus is simply to compare the performance that can be realized for a given configuration. This corresponds to the situation that often occurs in practice, where one has limited control over the possible locations for sources and sensors. Given this objective, for this theoretical development a single primary source and a single control source are also assumed to simplify the notation.

The pressure field in the rectangular enclosure can be represented in terms of the modes of the enclosure as

$$p(\vec{x}) = \sum_{N=0}^{\infty} (A_N + B_N Q_c) \Psi_N(\vec{x}) \ . \qquad (1)$$

Here, N denotes a triple sum over the indices (l, m, n) corresponding to the x-, y-, and z-directions. The functions Ψ_N correspond to the eigenfunctions of the enclosure, Q designates the complex control source strength, and the coefficients A_N and B_N are the modal coefficients associated with the primary field and the secondary control field, respectively. (The source strength of the primary source is included in the A_N coefficients.) The objective of the active control system is to optimize the value of the source strength, Q_c, so as to minimize a chosen performance function.

In this work, three different performance functions for the control system were investigated to compare their global performance. The first performance function corresponds to the global potential energy in the enclosure. This function was suggested by Nelson, *et al.*[1], since it provides a global measure of the energy in the field. While this approach is attractive for analytical work, it is problematic for experimental implementation, due to the lack of appropriate sensors to obtain a global measure of the potential energy. The second performance function investigated corresponds to the squared pressure at a discrete location(s). This is the approach most often taken in practice, and corresponds to minimizing the pressure magnitude at discrete points in the enclosure. While this approach lends itself well to experimental implementation, it often leads to the production of localized zones of silence, rather than the broad global attenuation often desired. The third performance function investigated corresponds to minimizing the total energy density at a discrete location(s). This approach also makes use of a local measurement, but the measurement of energy density potentially yields more global information than is obtained from a pressure measurement.

These three performance functions can be expressed as:

$$
\begin{aligned}
J_{pe} &= \int_V \frac{p^2}{2\rho c^2}\, dV \\
J_p &= \sum_{i=1}^{I} p^2(\vec{x}_i) \\
J_{ed} &= \sum_{i=1}^{I} \frac{p^2(\vec{x}_i)}{2\rho c^2} + \frac{\rho}{2}\vec{v}(\vec{x}_i)\cdot\vec{v}(\vec{x}_i)\ .
\end{aligned}
\tag{2}
$$

Here, the subscript *pe* refers to potential energy, the subscript *p* refers to the squared pressure, and the subscript *ed* refers to the energy density, and *I* indicates the number of error sensors used.

Using the expression for the pressure given in Eq. (1), these three performance functions can be minimized to yield the optimal control source strengths. The results of this minimization can be expressed as[4]:

$$
\begin{aligned}
Q_{c,pe} &= -\frac{\sum_{N=0}^{\infty} B_N^* A_N}{\sum_{N=0}^{\infty} B_N^* B_N} \\
Q_{c,p} &= -\frac{\sum_{i=1}^{I}\sum_{N=0}^{\infty} A_N \Psi_N(\vec{x}_i)}{\sum_{i=1}^{I}\sum_{N=0}^{\infty} B_N \Psi_N(\vec{x}_i)} \\
Q_{c,ed} &= -\frac{\sum_{i=1}^{I}\sum_{N=0}^{\infty}\sum_{M=0}^{\infty} A_N B_M^* \left[\Psi_N(\vec{x}_i)\Psi_M(\vec{x}_i) + \frac{1}{k^2}\nabla\Psi_N(\vec{x}_i)\cdot\nabla\Psi_M(\vec{x}_i)\right]}{\sum_{i=1}^{I}\sum_{N=0}^{\infty}\sum_{M=0}^{\infty} B_N B_M^* \left[\Psi_N(\vec{x}_i)\Psi_M(\vec{x}_i) + \frac{1}{k^2}\nabla\Psi_N(\vec{x}_i)\cdot\nabla\Psi_M(\vec{x}_i)\right]}
\end{aligned}
\tag{3}
$$

Looking at these three control results indicates that controlling the energy density would give the same controlled field if

$$
\sum_{i=1}^{I}\left[\Psi_N(\vec{x}_i)\Psi_M(\vec{x}_i) + \frac{1}{k^2}\nabla\Psi_N(\vec{x}_i)\cdot\nabla\Psi_M(\vec{x}_i)\right] = \delta_{NM} \tag{4}
$$

This equality is not true in general, but the results obtained do confirm that the control source strength obtained by minimizing the energy density generally more closely approximates the source strength for minimizing the global potential energy than when minimizing the square pressure.

4.2 Numerical Model and Results

One of the major accomplishments of the study has been the development of a model of the control approach. This model has aided greatly in developing a better understanding of the control mechanisms associated with controlling the energy density. The model is based on a modal representation of the interior field. With this representation, the acoustic pressure can be represented as a summation of the modes, and related quantities such as the global potential energy and the energy density can also be represented in terms of the acoustic modes. The enclosure used in the model corresponds to a rigid rectangular enclosure, with dimensions 1.93 m × 1.22 m × 1.54 m. These dimensions correspond to an enclosure at The Pennsylvania State University that was used for experimental verification of the results. The resulting expression for the modes of the enclosure is given by

$$\Psi_N(\vec{x}_i) = \cos\left(\frac{l\pi x_i}{L_x}\right)\cos\left(\frac{m\pi y_i}{L_y}\right)\cos\left(\frac{n\pi z_i}{L_z}\right) \tag{5}$$

where L_x, L_y, L_z are the dimensions of the enclosure along the three axes.

The numerical model allows the user to specify the number of modes to be included in the model. It was found empirically that retaining one thousand modes in the model yields convergence for the modal summations. (Retaining two hundred modes produces results within about 1 dB of the converged solution, and was often used to quickly obtain general results.) The model also allows the user to specify the dimensions of the enclosure, the damping coefficient, and the locations of the sources and sensors. Any number of sensors and sources can be used, with the current limitation that the number of sensors must be greater than or equal to the number of sources. It is planned to modify the model in the future to be able to remove this restriction.

To look at the effect of controlling the energy density rather than the squared pressure, there are several ways in which one can analyze the results. A global measure of the control is given by the potential energy in the enclosure, both before and after the control is applied. Thus, one of the options with the model is to determine the potential energy in the enclosure as a function of frequency for the cases of no control, minimizing the potential energy (which can be done numerically, but not experimentally), minimizing the squared pressure, and minimizing the energy density. The case of minimizing the potential energy is often considered to be the optimal result, since it represents the least amount of global energy in the enclosure. Figure 1 shows a typical result obtained from the model for determining the potential energy as a function of frequency in the enclosure. For these results, a single primary source was arbitrarily located at $(x,y,z) = (0.1,0.4,0.4)$, a single control source was located at $(x,y,z) = (1.4,1.0,1.0)$, and the error sensor was located at

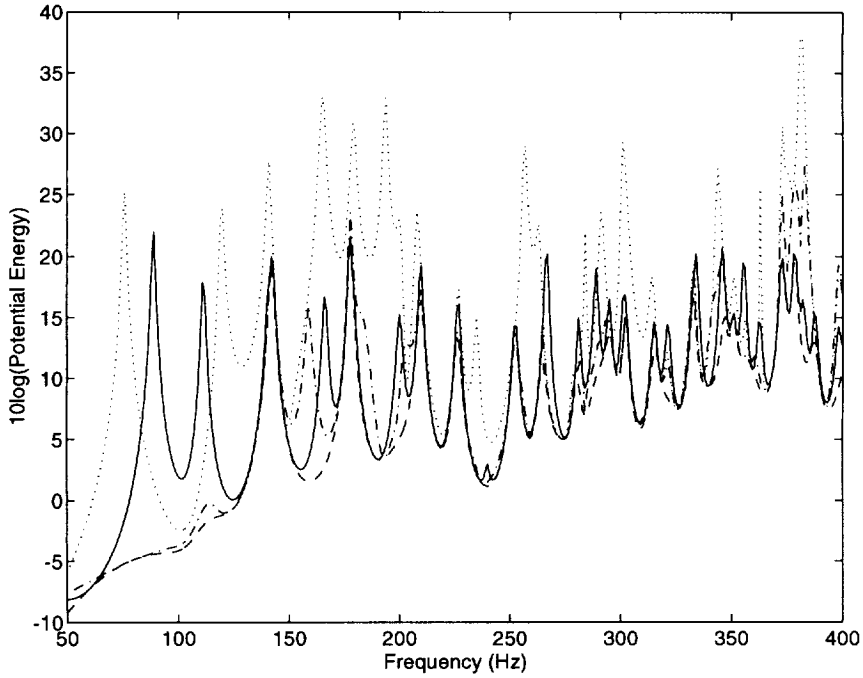

Figure 1. Potential energy in the enclosure. —— no control; - - - potential energy; ····· squared pressure; -·-· energy density.

$(x,y,z) = (1.2,0.6,0.6)$. As mentioned previously, no attempt was made to optimize these locations.

From these results, it can be seen that minimizing the potential energy yields the lowest global energy, as is to be expected. However, minimizing the energy density at the single point chosen yields potential energy results that are comparable to minimizing the potential energy at most of the frequencies shown here. On the other hand, minimizing the squared pressure leads to an increase in the global potential energy in the enclosure at most frequencies. This can be seen more clearly in Figure 2, which shows the attenuation in the potential energy that is achieved using each of the three control approaches. The negative values of attenuation at most frequencies for the squared pressure control indicate an increase in the energy in the enclosure, while controlling the energy density provides attenuation of the global field that approximates the control of potential energy reasonably well.

An additional insight that was obtained through use of the model was the sensitivity of the control achieved on the error sensor location with the various methods. Since the global potential energy represents an integration of the potential energy density over the entire enclosure, the control achieved by minimizing the potential energy does not depend on sensor location. For reference, the attenuation achieved with this method is shown in Figure 3. If one chooses to minimize the squared pressure or energy density, the attenuation achieved generally depends on error sensor location. To investigate this, ten sensor locations were chosen along a line through the enclosure that roughly

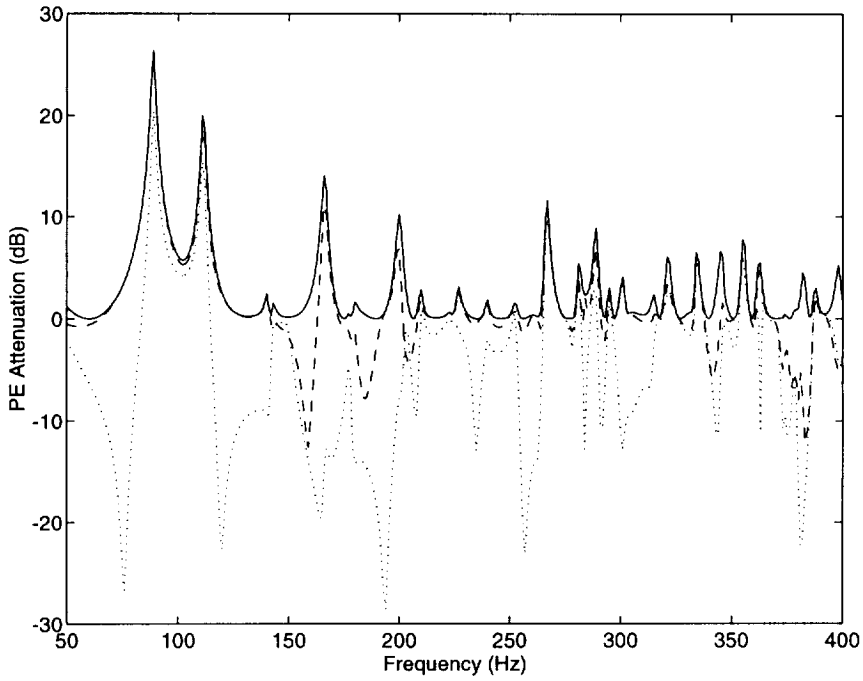

Figure 2. Attenuation of potential energy in the enclosure. —— no control; - - - potential energy; ····· squared pressure; -·-· energy density.

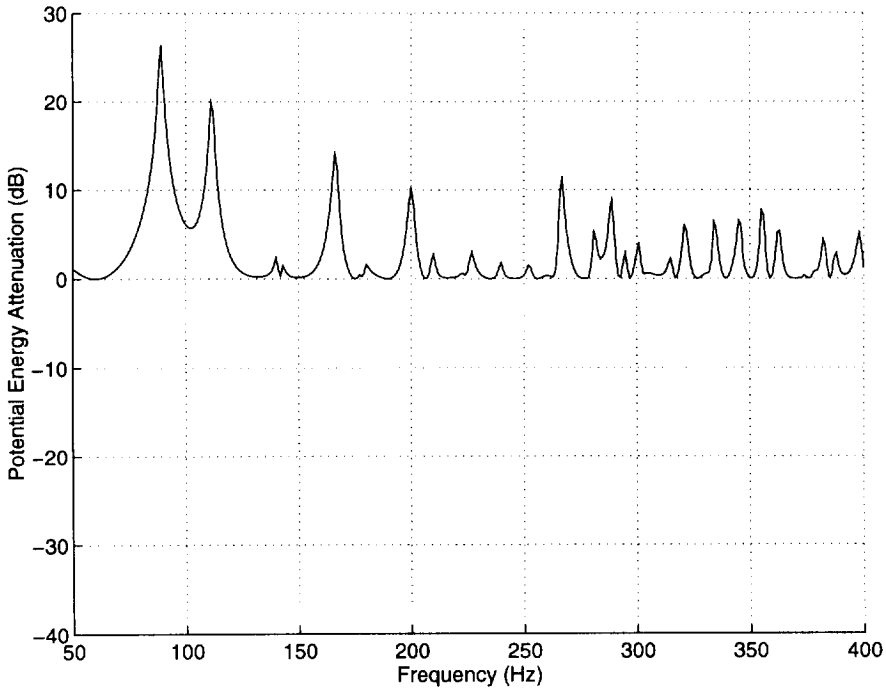

Figure 3. Attenuation of the potential energy in the enclosure, when minimizing the potential energy.

corresponds to a diagonal through the enclosure. (Points exactly along the diagonal were not used to avoid any potential anomalies in the results.) Figure 4 shows an overlay of the ten attenuation curves as a function of frequency for the ten sensor locations when minimizing the squared pressure. It is apparent that there are wide discrepancies in the attenuation achieved as the sensor is placed at different locations. Figure 5 shows the same results for the case of minimizing the energy density. It can be seen that the attenuation achieved when minimizing the energy density also depends on the sensor location, but the attenuation achieved is significantly more uniform with sensor location when minimizing energy density than when minimizing squared pressure. Most of the curves for minimizing the energy density tend to conform reasonably well with the attenuation achieved when minimizing the global potential energy. These results suggest that if one is constrained in where the sensors can be located, there will be a greater probability of achieving near optimal control by minimizing energy density than by minimizing squared pressure.

Some insight into the reasons for the behavior described previously can be obtained by considering the spatial dependence of the modes in the enclosure, both in terms of pressure and in terms of the energy density. If one considers a single mode to be dominant, the squared pressure in the field can be expressed approximately as

$$|p(\vec{r})|^2 = \cos^2(k_x x)\cos^2(k_y y)\cos^2(k_z z) \tag{6}$$

where the amplitude of the mode has been normalized to unity. In this expression, $k_x = m\pi/L_x$, $k_y = n\pi/L_y$, and $k_z = l\pi/L_z$. Similarly, the energy density in the field can be expressed as

$$\begin{aligned} w = {} & \cos^2(k_x x)\cos^2(k_y y)\cos^2(k_z z) + \frac{1}{k^2}\left[k_x^2 \sin^2(k_x x)\cos^2(k_y y)\cos^2(k_z z)\right. \\ & \left. + k_y^2 \cos^2(k_x x)\sin^2(k_y y)\cos^2(k_z z) + k_z^2 \cos^2(k_x x)\cos^2(k_y y)\sin^2(k_z z)\right] \end{aligned} \tag{7}$$

In terms of the pressure field, there are nodal planes that exist wherever the cosine functions go to zero. Thus, for the (m,n,l) mode, there will be a total of $m+n+l$ nodal planes that represent locations where the error sensors will be unable to detect the dominant mode, and poor control results can be expected. However, if one is minimizing the energy density, the spatial variability of the energy density field is significantly different. For example, for an axial mode (where, for example n and l are zero) the energy density will be uniform throughout the enclosure, and the control achieved will be nearly independent of error sensor location. For the cases of tangential and oblique modes, an investigation of Eq. (8) reveals that instead of having nodal planes, as in the case of the pressure field, there are now nodal lines that occur at the intersection of two pressure nodal planes. As a result, the regions of the enclosure that represent poor sensor locations are much more restricted for the energy density field than for the pressure field. This spatial dependence can be seen in Figure 6 for the case of an axial mode, and in Figure 7 for the case of a tangential mode. Given this difference in spatial dependence, it can be seen that there will be noticeably less sensitivity to error sensor location when minimizing the energy density, rather than the squared pressure. It should be mentioned that these results may be modified to some extent when there are multiple significant

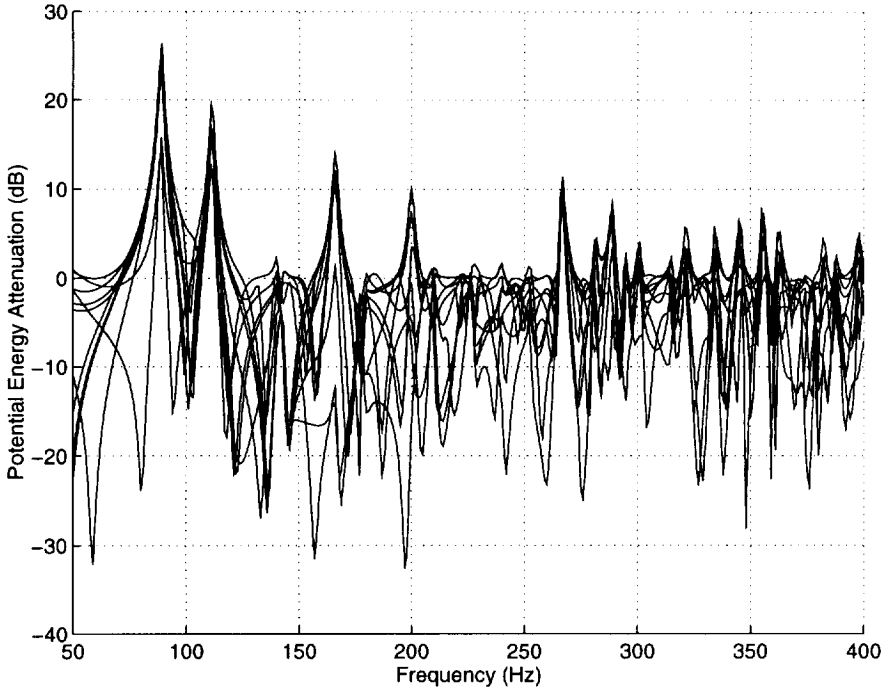

Figure 4. Attenuation of the potential energy in the enclosure, when minimizing the squared pressure at 10 different locations.

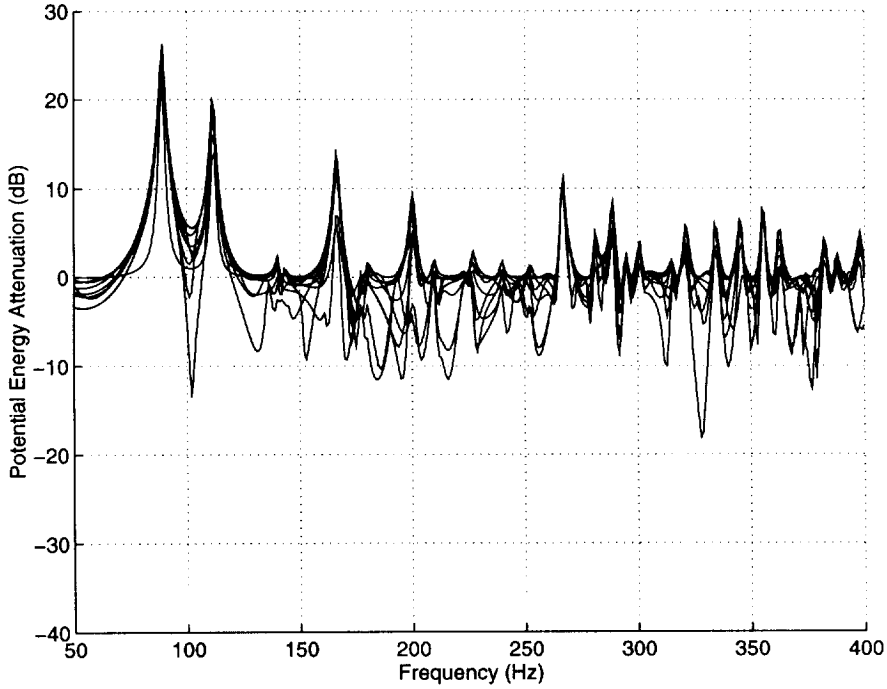

Figure 5. Attenuation of the potential energy in the enclosure, when minimizing the energy density at 10 different locations.

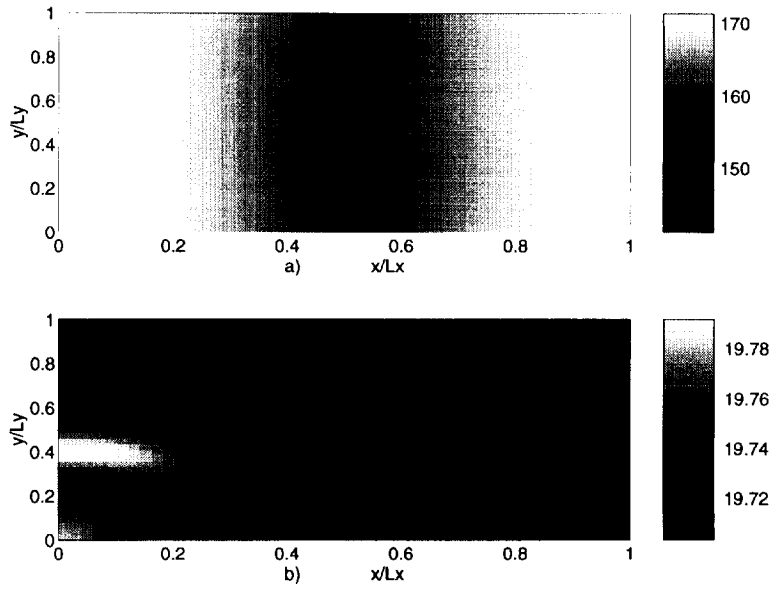

Figure 6. Spatial dependence of the relative level (dB) of the acoustic field for the (1,0,0) mode (88.9 Hz): a) Pressure; b) Energy density.

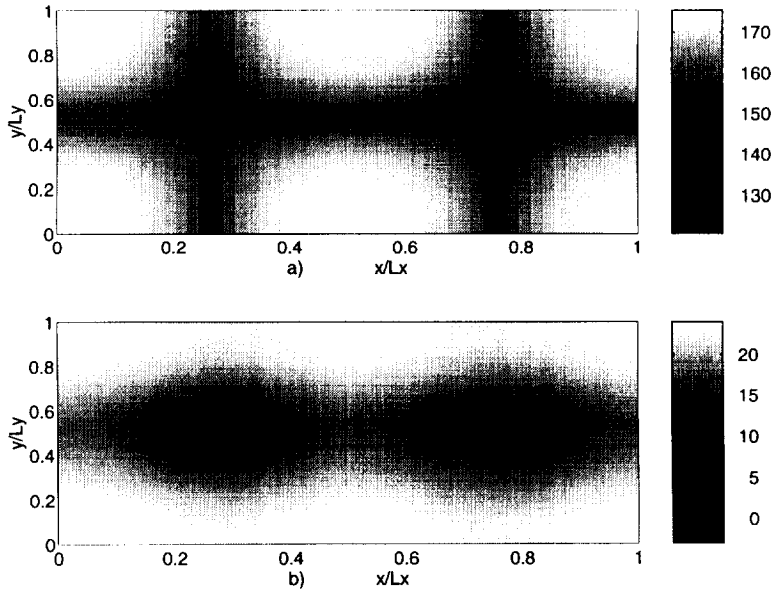

Figure 7. Spatial dependence of the relative level (dB) of the acoustic field for the (2,1,0) mode (210 Hz): a) Pressure; b) Energy density.

modes contributing to the field, since the multiple modes can combine in such a way as to create a local minimum in either the pressure or the energy density, even if the sensor is not on a nodal surface of the modes.

In addition to looking at the global potential energy as a function of frequency, it is also possible with the model to investigate the spatial dependence of the pressure and energy density fields for a given frequency. This is useful for investigating the field that results using the various control approaches, and identifying features such as localized areas of attenuation and effects due to good or poor source/sensor locations. It is conceivable that two control methods could result in the same global energy within the enclosure, but that the spatial dependence of the field may be more desirable with one approach than the other. This feature of the model allows the user to investigate these issues.

As an example of the spatial dependence of the acoustic field, consider the resonance peak located at 166 Hz in Figure 1, which corresponds to the (1,1,0) mode. It can be seen that under these conditions, minimizing the squared pressure leads to a significant increase in the potential energy in the enclosure, even though the pressure at the error sensor is significantly attenuated. On the other hand, minimizing the energy density or the global potential energy leads to a reduction of the total potential energy in the enclosure in the range of 11-14 dB. Figures 8 and 9 show the relative sound pressure level for two different cross-sectional planes of the enclosure, given by $y = 0.8$ m and $y = 1.0$ m. For the (1,1,0) mode, the error sensor (located at $y = 0.6$ m) is near the nodal plane of the mode given by $y = 0.61$ m. As a result, if the squared pressure is controlled, the error sensor is largely incapable of detecting the dominant mode in the enclosure, and as a consequence, the control solution results in a general increase in the sound pressure levels throughout the enclosure. The effect of the control is to attenuate secondary modes, while amplifying the already dominant mode. On the other hand, since the energy density control approach is also sensitive to velocity components of the modes, it is capable of detecting the dominant mode in the enclosure, and yields a much more satisfactory solution. It can also be seen that the spatial dependence of the pressure field when minimizing the energy density is similar in nature to the spatial dependence when minimizing the global potential energy. There are, however, some differences, which leads to the difference in overall attenuation of about 3 dB.

4.2.1 Multiple Sensor Results:

As part of the numerical research, the use of multiple control sources and/or sensors was investigated. The one limitation was that the number of sensors was constrained to be greater than or equal to the number of sources. The results that were obtained were not unexpected and confirmed results obtained by others in terms of minimizing the squared pressure in the enclosure. The results do, however, provide some interesting insight into the issue of controlling the energy density vs. controlling the squared pressure.

An example of using multiple sources is shown in Figures 10-12. For these results, twelve randomly located microphones were used for minimizing the squared pressure, while three energy density sensors (located at the first three microphone locations) were used for minimizing the energy density. Figure 10 shows the results using a single (poorly located) control source, while Figure 11

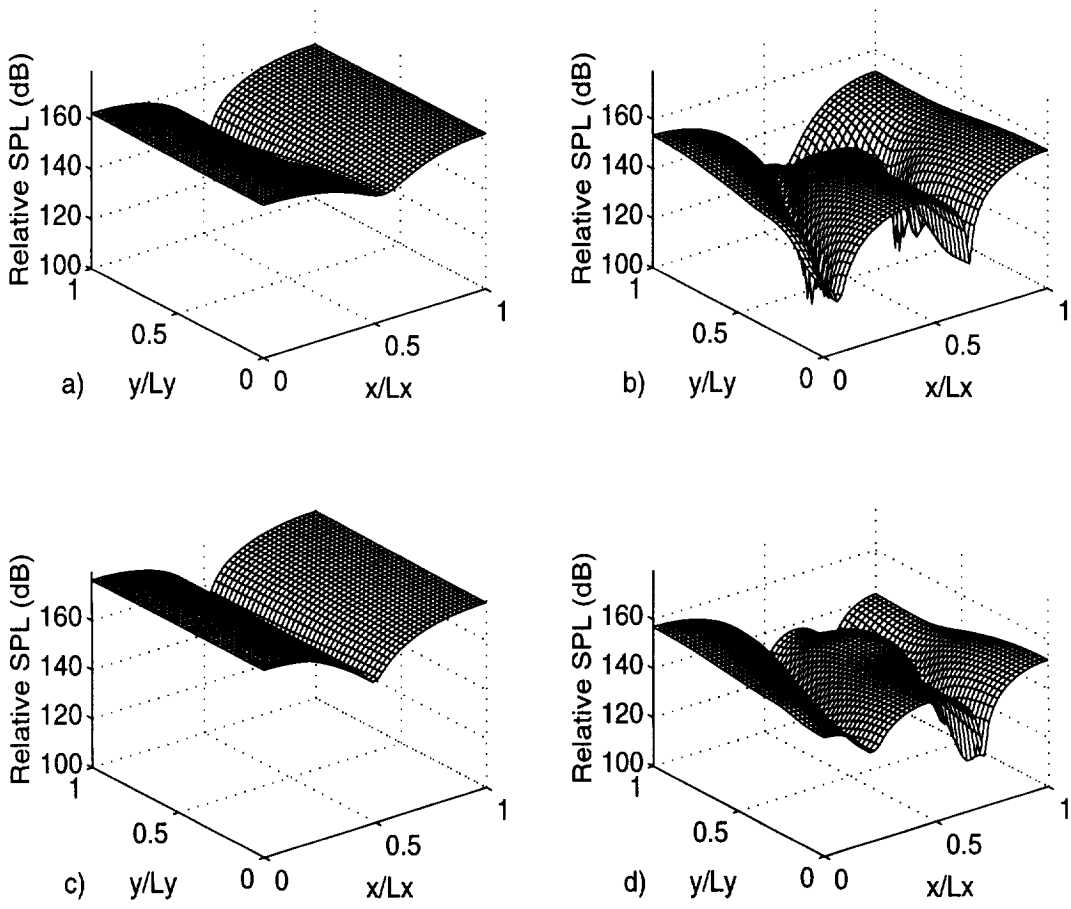

Figure 8. Relative sound pressure level in the z = 0.8 m plane: a) No control; b) Potential energy minimized; c) Squared pressure minimized; d) Energy density minimized.

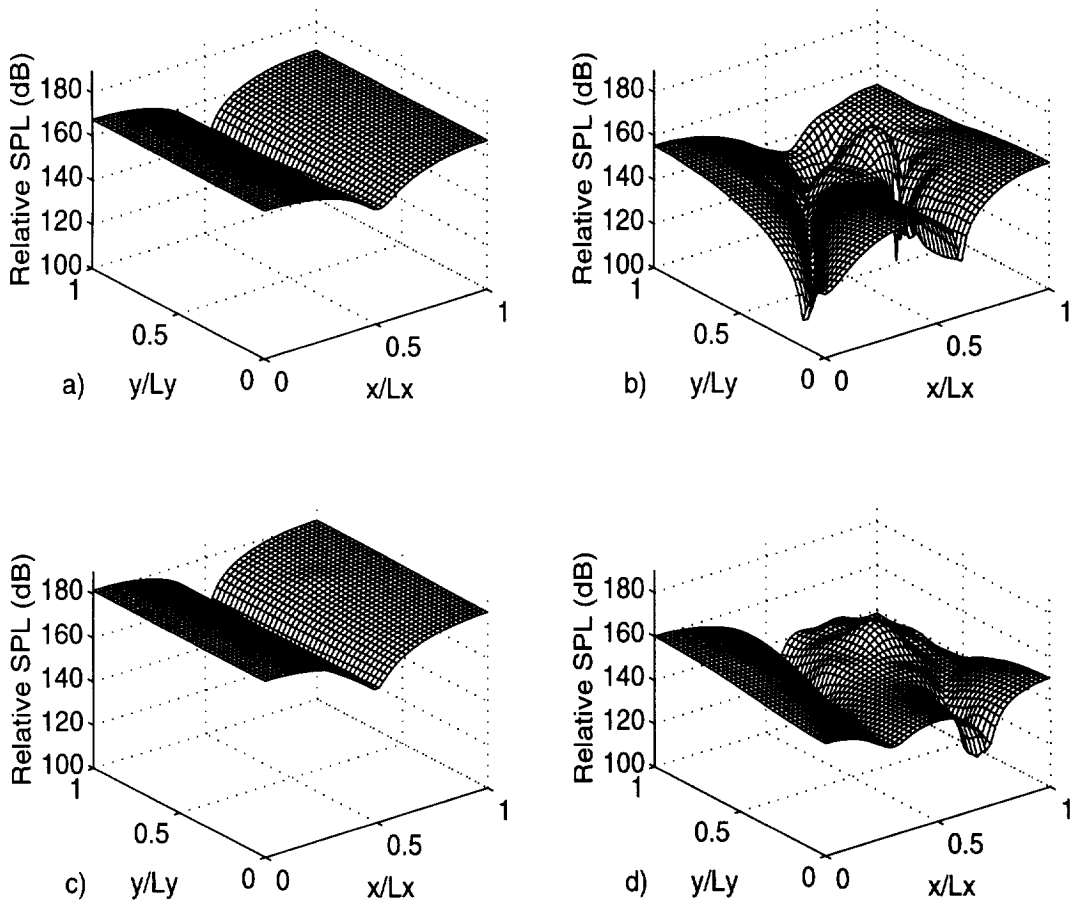

Figure 9. Relative sound pressure level in the z = 1.0 m plane: a) No control; b) Potential energy minimized; c) Squared pressure minimized; d) Energy density minimized.

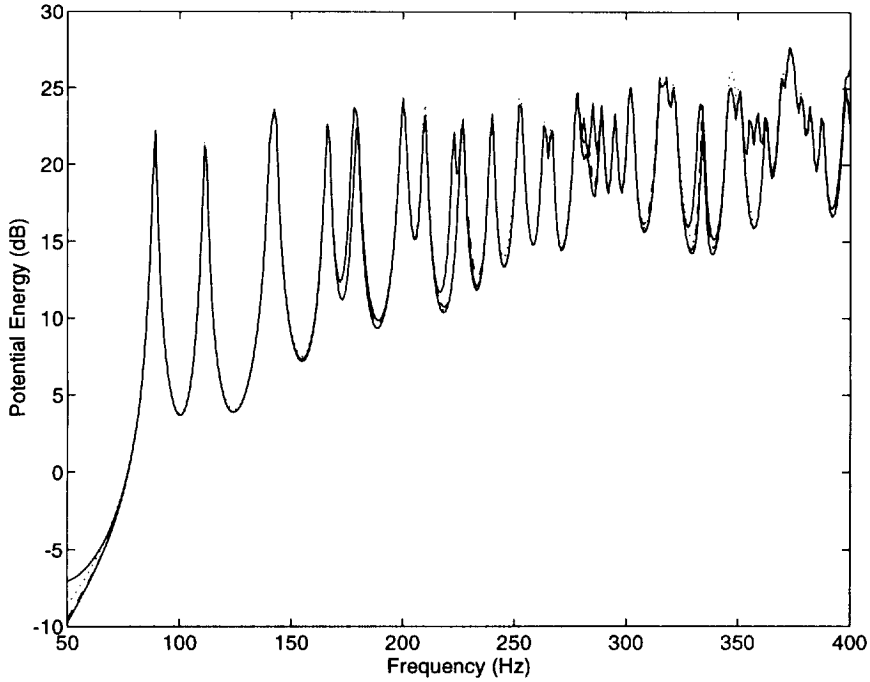

Figure 10. Potential energy in the enclosure with one control source, located at (.501,.501,.501). —— (upper) no control; —— (lower) potential energy; - - - squared pressure; ····· energy density.

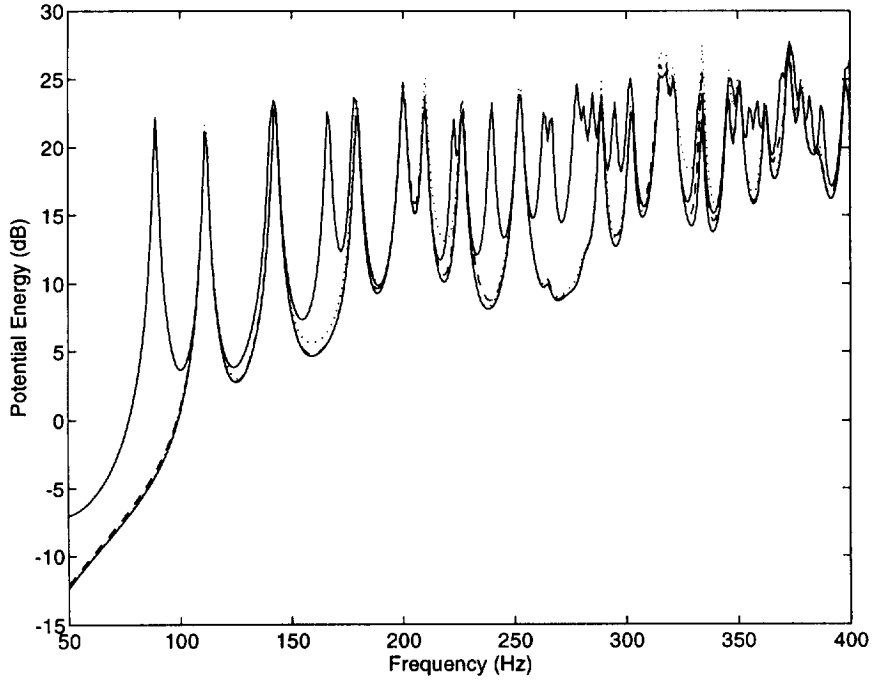

Figure 11. Potential energy in the enclosure with two control sources, located at (.501,.501,.501) and (.251,.501,.330). —— (upper) no control; —— (lower) potential energy; - - - squared pressure; ····· energy density.

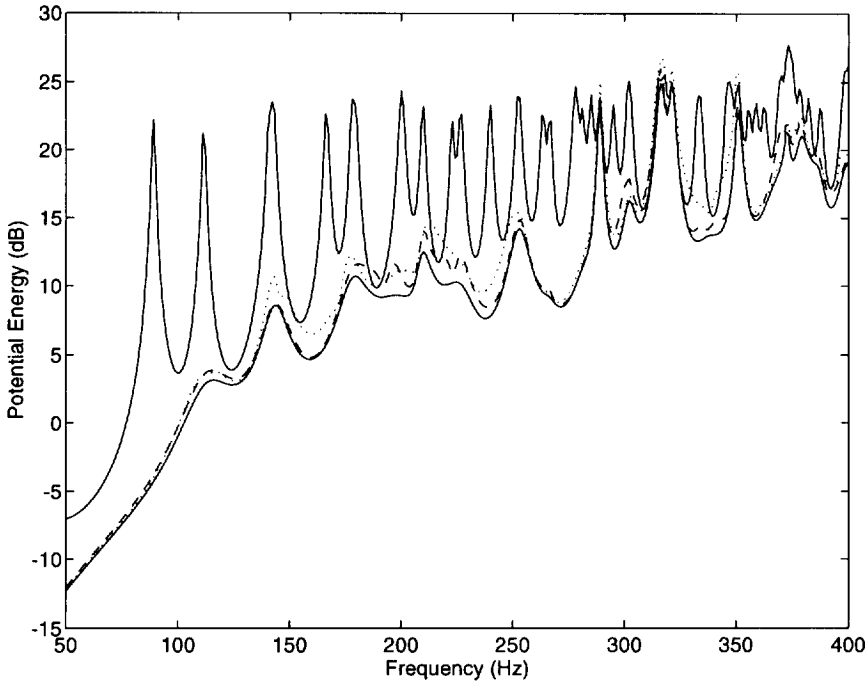

Figure 12. Potential energy in the enclosure with three control sources, located at (.501,.501,.501), (.251,.501,.330), and (.831,.345,.831). —— (upper) no control; —— (lower) potential energy; - - - squared pressure; ····· energy density.

shows the results for two control sources, and Figure 12 shows the results for three control sources. Also, in these figures, dimensions given are normalized by the dimensions of the enclosures. For the case of the single control source, it can be seen that very little control can be obtained, since the normalized source location of (.501,.501,.501) corresponds to a nodal location for almost every mode of the enclosure, such that the control source is unable to excite the required modes. Figures 11 and 12 indicate that as the number of sources is increased, improved control can be expected. In fact, for this configuration, one can see that three control sources (effectively two control sources) are capable of providing reasonable control at nearly all of the frequencies shown. It can also be seen that the amount of attenuation achieved by minimizing the energy density at three energy density sensors is very comparable to the attenuation achieved by minimizing the squared pressure at twelve sensors, and that both methods reasonably approximate the attenuation that can be achieved by minimizing the global potential energy. Since an "energy density sensor" requires multiple sensors, the total number of sensors required for three energy density sensors is comparable to the twelve pressure sensors used. However, from a control perspective, there are still significant advantages to minimizing the energy density, since there are fewer error signals to be minimized, which reduces the complexity of the control system. In addition, the results obtained indicate that minimizing the energy density is significantly less sensitive to error sensor location.

Figures 13-15 provide representative results for changing the number of error sensors. For these results, a single control source located at (.711,.851,.330) is assumed, and the number of error

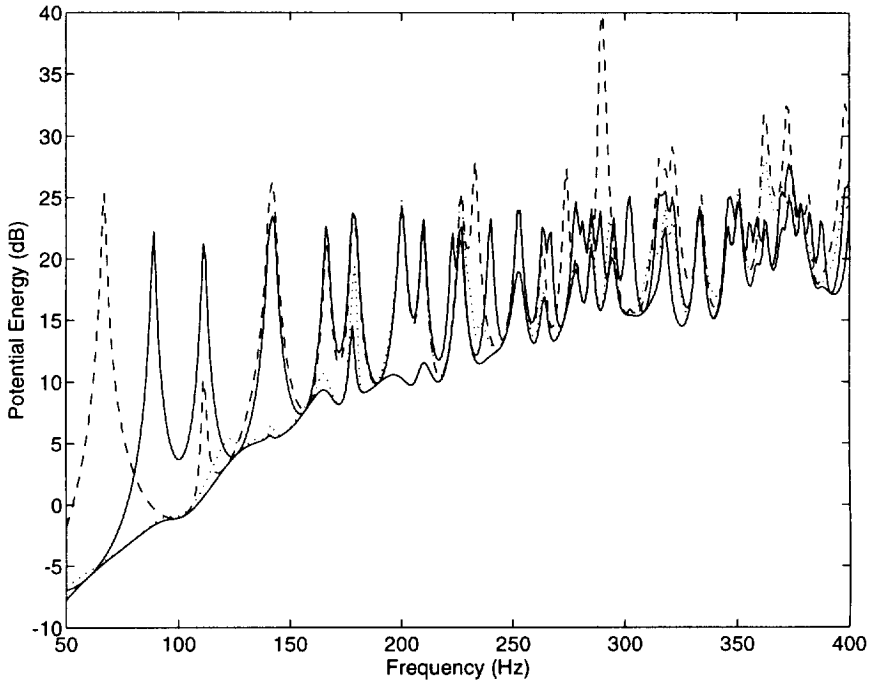

Figure 13. Potential energy in the enclosure with one error sensor, located at (.751,.501,.501). —— (upper) no control; —— (lower) potential energy; - - - squared pressure; ····· energy density.

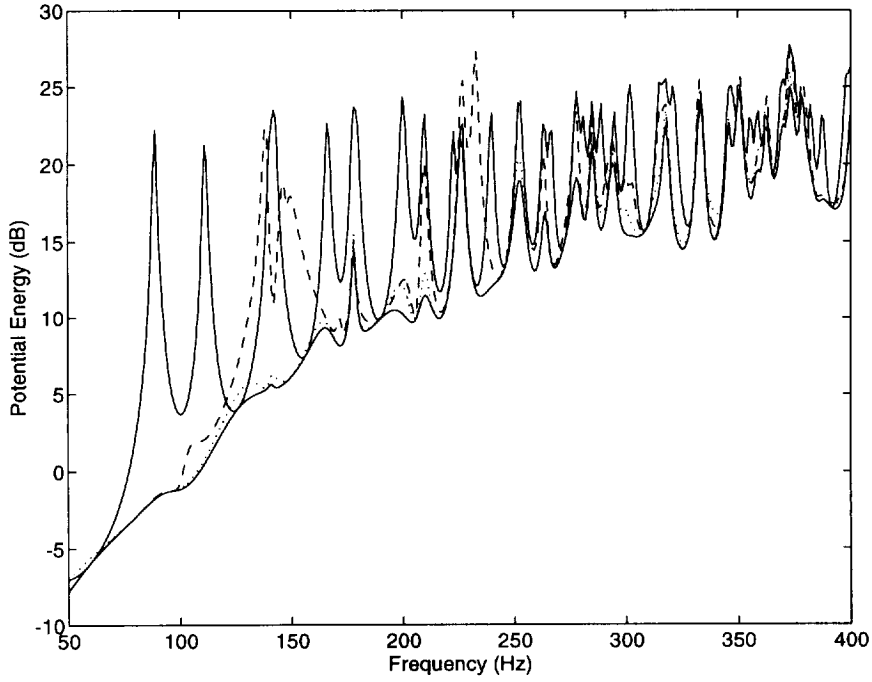

Figure 14. Potential energy in the enclosure with two error sensors, located at (.751,.501,.501) and (.256,.256,.751). —— (upper) no control; —— (lower) potential energy; - - - squared pressure; ····· energy density.

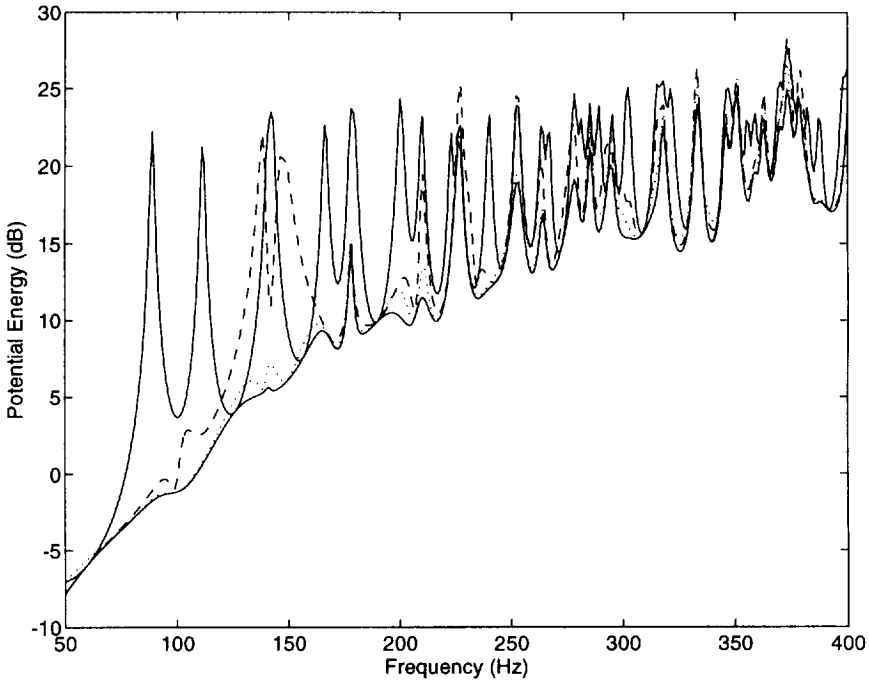

Figure 15. Potential energy in the enclosure with three error sensors located at (.751,.501,.501), (.256,.256,.751) and (.241,.313,.781). —— (upper) no control; —— (lower) potential energy; - - - squared pressure; ····· energy density.

sensors is varied from one to three. Figure 13 shows the results obtained for a single sensor location. It can be seen that there are a number of frequencies where minimizing the squared pressure leads to an increase in the global potential energy, due to the poor location of the sensor for those frequencies. On the other hand, with just a single energy density sensor, one already achieves control which approximates minimizing the global potential energy at most frequencies shown here. Adding a second sensor (Figure 14) leads to improved performance in terms of minimizing the squared pressure, but there are still a number of frequencies that cannot be effective controlled. There is also some improvement in terms of minimizing the energy density, but the improvements are not very dramatic, since even a single energy density sensor provided rather good results. Adding a third sensor (Figure 15) continues this trend, with some improvements in terms of minimizing the squared pressure, and very little difference in terms of minimizing the energy density.

In conclusion, the results of the numerical research have indicated that from a sensor perspective, if one has a fixed number of sensor sites, one can nearly always achieve better performance by minimizing the energy density than by minimizing the squared pressure. However, since an energy density sensor requires multiple sensors, it is also reasonable to look at this issue in terms of an equal number of sensors used, rather than sensor sites. If this comparison is made, the results indicate than one will generally achieve about the same amount of global attenuation when minimizing the energy density as when minimizing the squared pressure. However, as pointed

out earlier, when minimizing the energy density, there is still the advantage that the attenuation achieved is not as sensitive to sensor location. As well, since there are fewer error signals, there is a potential to achieve reduced controller complexity for the implementation.

4.3 Experimental Verification

An important part of the research consisted of developing the algorithms and hardware necessary to be able to experimentally verify the numerical results. The rectangular enclosure used for this study existed previously and consisted of a rectangular plywood box of dimensions 1.93 m × 1.22 m × 1.54 m. The plywood walls consisted of 19 mm (¾") plywood, which was reinforced with a grid of braces on the exterior surfaces. The primary sound field was generated using a single Bose 101 loudspeaker, and an additional Bose 101 loudspeaker(s) was used for the secondary control source(s).

To investigate the spatial dependence of the acoustic field, an array of nine Lectret 1207A microphones were mounted on a boom that could be traversed throughout the enclosure to measure the acoustic field. The levels at each microphone location were recorded, from which the three-dimensional dependence of the field could be determined.

Two control approaches were implemented experimentally: minimization of squared pressure, and minimization of energy density. To implement these methods required the development of a three-dimensional "energy density sensor", as well as the control algorithms. Each of these will be discussed in some detail.

4.3.1. Energy Density Sensor

To implement the approach of minimizing the energy density, it is necessary to not only sense the acoustic pressure, but also to sense the acoustic particle velocity. Several possible approaches were investigated for sensing the particle velocity. The approach that was finally used consists of using finite differences with two closely spaced microphones in each of the three orthogonal directions, in the same spirit as is used to measure acoustic intensity. This approach follows directly from Euler's equation, given as

$$\begin{aligned} v_m(n) &= \frac{-1}{\rho} \int \frac{\partial p}{\partial x_m} dn \\ &\approx \frac{-1}{\rho \, \Delta x_m} \int \left[p_2(n) - p_1(n) \right] dn \ , \end{aligned} \tag{8}$$

where Δx_m is the spacing between two closely spaced microphones in the x_m direction.

It was desired to develop a relatively inexpensive probe to measure the energy density, since

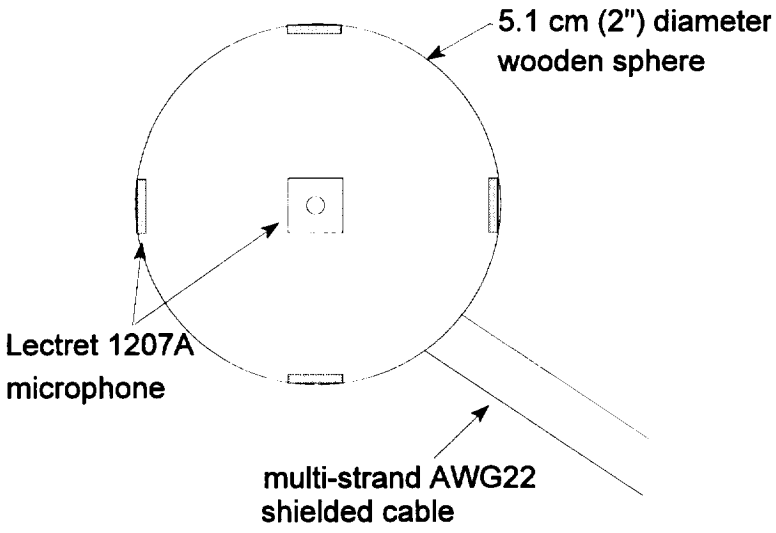

Figure 16. Schematic of the energy density sensor probe.

it would be undesirable for any practical implementation to rely on expensive phase-matched pairs of microphones. This was accomplished using six Lectret 1207A microphones that were flush mounted in a 5.1 cm wooden ball[5], as shown in Figure 16. The three pairs of microphones were mounted on opposite sides of the sphere, so as to be able to estimate the three orthogonal components of the particle velocity. This type of spherical probe has been discussed previously by Elko[6], and was shown to have favorable characteristics with respect to the finite difference and finite sum bias errors. The inside of the wooden ball was hollowed out, and a small circuit board was mounted inside the ball. Six noninverting pre-amplifiers were mounted on the circuit board to buffer the outputs from the microphone and to provide voltage gain. The amplified signals from the six microphones are transmitted by means of a shielded cable to a second set of noninverting amplifiers located outside of the enclosure. These amplifiers have variable resistors associated with them that allow the gains of the amplifiers to be adjusted for microphone calibration purposes. A schematic of the electronics associated with each microphone can be seen in Figure 17.

Each of the six microphones was calibrated by placing each microphone into one side of a small calibration chamber, along with a B&K Type 4133 microphone, as shown in Figure 18. The gain for the microphone was then adjusted so that the output level was 50 dB higher than that of the B&K microphone. The result of this process was that the microphones were all calibrated to provide an output of 1 Vrms @ 94 dB re 20μPa at 100 Hz. The Lectret microphones were found to provide a stable, linear response up to levels greater than 110 dB re 20μPa, with a flat phase and amplitude response. The phase response is within ±1° at 100 Hz for all six microphones, and is within that range for all frequencies of interest above 100 Hz.

With the energy density probe, the three pairs of microphones could be used to provide the finite difference estimation of the pressure gradient in Eq. 8. To obtain the velocity components,

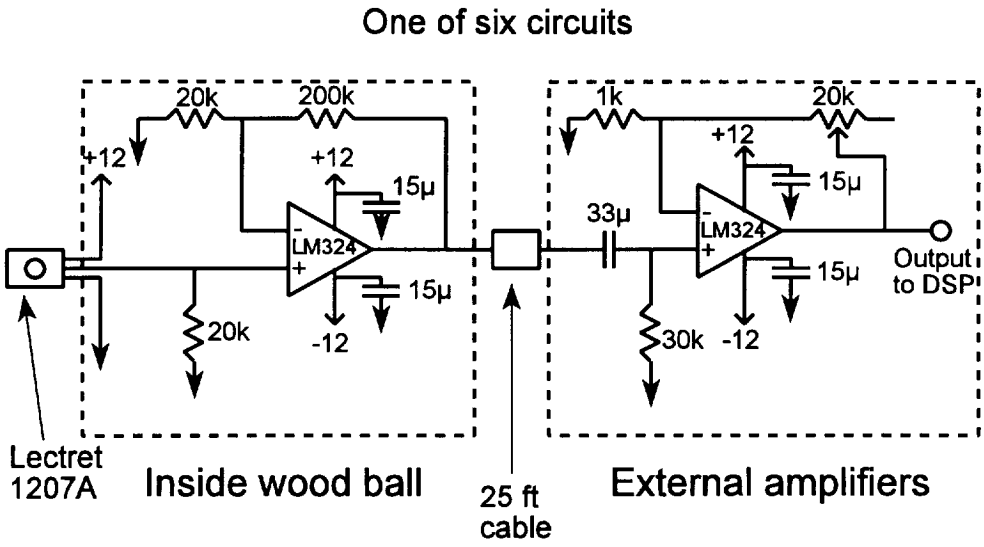

Figure 17. Schematic of the electronics for each microphone in the energy density sensor.

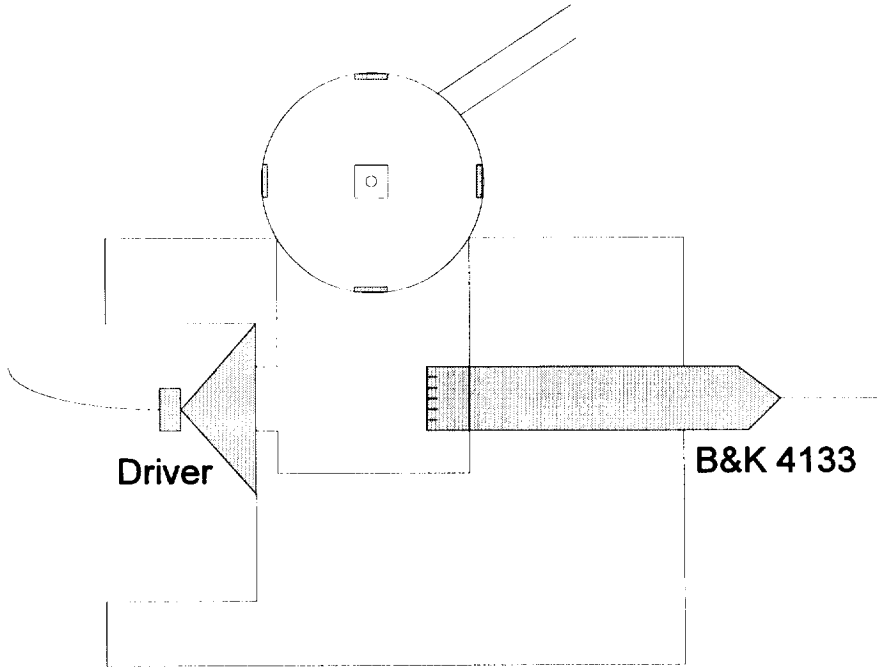

Figure 18. Calibration chamber used to calibrate the energy density probe.

it is also necessary to perform a time integration of the pressure difference. This has been done both digitally and with an analog circuit, and both methods perform acceptably. However, it was found that generally, the digital integration tended to provide a more stable signal. For the results presented here, a digital integration scheme was implemented, in accordance with the work presented by Hodges, *et al.*[7] With this approach, the six microphone signals are input to the DSP board, where the average of the six pressure signals is used as an estimate of the pressure at the sensor location, and the time integration of the pressure differences in each direction is used to obtain the particle velocity components, as given in Eq. 8.

4.3.2 Control Algorithms

For both control methods, the control algorithm was based on the filtered-*x* LMS algorithm, developed by Widrow and Stearns[8]. With this control approach, the control filter is represented by an adaptive finite impulse response (FIR) filter that is updated at each time iteration, based on the measured error signals. For the method of minimizing the squared pressure, the filter coefficients are updated according to

$$w_i(n+1) = w_i(n) - \mu e(n) r(n-i) \ , \tag{9}$$

where $w_i(n)$ represents the ith coefficient of the control filter at the discrete time n, μ is a convergence parameter chosen to maintain stability, $e(n)$ is the error signal (pressure) measured at the error microphone, and $r(n)$ is the filtered reference signal, obtained by passing the reference input signal through the transfer function from the controller output to the error sensor input. The last term in the update equation represent the negative gradient of the performance function (squared pressure). For the method of minimizing the energy density, the filter coefficients are again updated according to the negative gradient of the performance function. However, with the performance function now being the energy density, the update equation now takes the form of [3]

$$w_i(n+1) = w_i(n) - \mu \left(\sum_{m=1}^{3} \rho v_m(n) r_{vm}(n-i) + \frac{1}{\rho c^2} p(n) r_p(n-i) \right) \ . \tag{10}$$

In this equation, m = 1,2,3 corresponds to the x-, y-, z-direction, respectively, v_m is the velocity in the m direction, $r_{vm}(n)$ is the filtered reference signal obtained by passing the reference input signal through the transfer function from the controller output to the velocity component in the m direction at the error sensor, and $r_p(n)$ is the filtered reference signal obtained by passing the reference input signal through the transfer function from the controller output to the pressure at the error sensor.

For both methods, the update equation used required the reference input signal to be passed through one or more transfer functions from the controller output to the error sensor. This requires implementing a model of the required transfer function(s) within the controller, through which the reference input signal can be passed to obtain the necessary filtered reference signal(s). These transfer functions can either be measured *a priori* and stored in the DSP board, or they can be

estimated in real-time. For this work, the transfer functions were estimated in real-time, using the method developed previously by Sommerfeldt[9].

4.3.3. Experimental Results

To determine how the response of the experimental enclosure compared with the numerical results for the enclosure, one of the loudspeakers was placed in a corner of the enclosure, and a microphone was placed in another corner to measure the frequency response of the enclosure. The experimental response is shown in Figure 19. The resonance frequencies of the enclosure are in good agreement with the numerical predications, as can be seen in Table 1. There are some additional spectral peaks, for example at 51, 56.5, 147.5, 159, and 189 Hz, that do not match up with predicted frequencies. It is thought that these frequencies are associated with resonance frequencies of the enclosure walls, which are not completely rigid.

For these results, the two control schemes were each implemented and the acoustic field was scanned over multiple horizontal planes. The results were then compared with the predicted results obtained from the numerical model to compare the spatial dependence of the field and the overall attenuation levels achieved. Several of the results obtained will be discussed here.

Some of the results obtained for an excitation frequency of 88 Hz (1,0,0 mode) can be seen in Figures 20-23. These figures show both the numerical and experimental results for two of the horizontal planes that were scanned. For the numerical results, the pressure field was determined for the cases of no control, controlling the squared pressure, controlling the energy density, and controlling the global potential energy. For these results, the error sensor was located at (0.96, 0.19, 0.76) m. This location represents a poor choice for the error sensor location when controlling the squared pressure, since it is located very near to the nodal plane for the (1,0,0) mode. As a result, the dominant mode in the enclosure is not observed by the control system, and the overall levels in the enclosure go up when the control is implemented, even though the local pressure at the error sensor is attenuated. This effect is apparent in both the numerical and the experimental results. On the other hand, when the energy density is controlled, the energy density does not have a node at the error sensor location. As a result, the controller is able to sense the dominant mode in the enclosure without difficulty and achieve a global control effect. It can be observed from Figures 20-23 that the general agreement for the spatial dependence of the field is quite good. The effect of controlling the energy density for this frequency is to yield a pressure field that is relatively uniform throughout the enclosure, and at a lower level than the uncontrolled field. It can also be seen from the numerical predictions that the energy density control closely approximates the control that would be achieved if one could minimize the global potential energy in the enclosure.

Figures 24-27 show the numerical and experimental results obtained for two of the horizontal planes scanned with an excitation frequency of 170 Hz (166.3 Hz numerically). This frequency corresponds to the (1,1,0) mode. For these results, the error sensor was located at (0.625, 0.615, 0.775) m. This location again represents a poor error sensor location for controlling the squared pressure, since it is located near the nodal plane at $y = 0.61$ m. As a result, the controller is not able

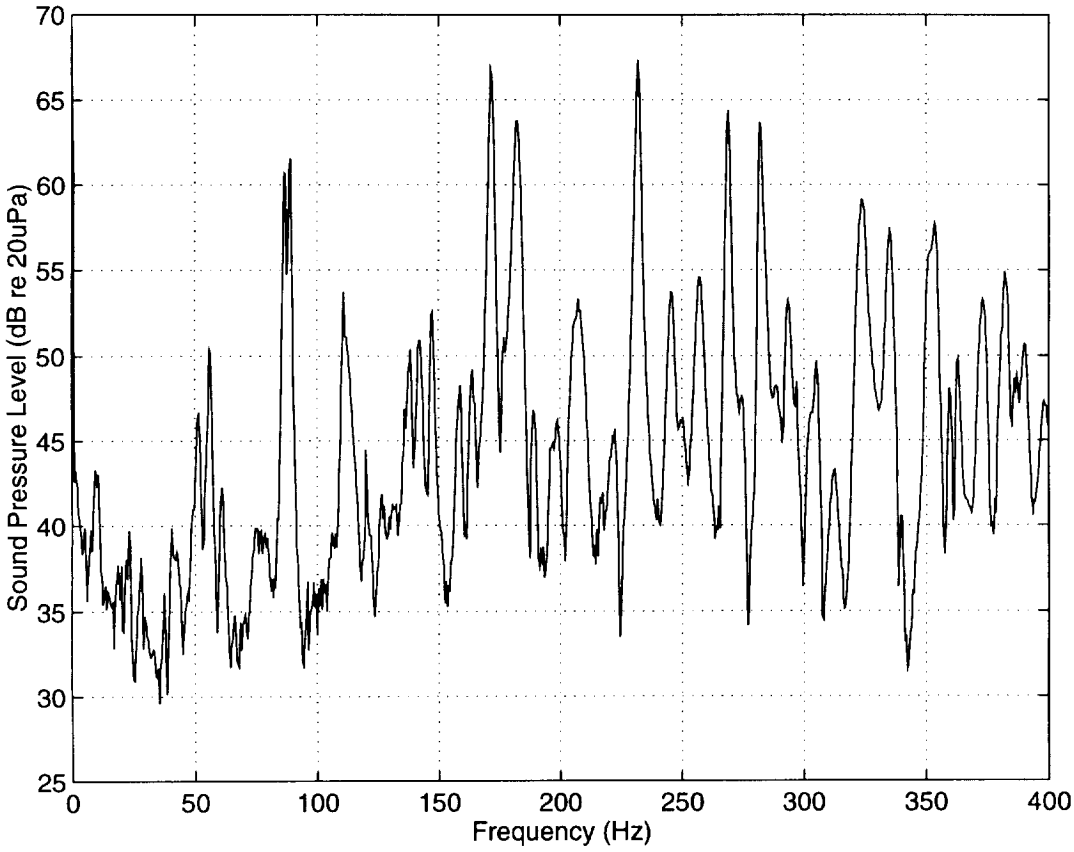

Figure 19. Measured frequency response of the enclosure.

Table 1. Numerical vs. Experimental Resonance Frequencies for the Enclosure.

Mode Number	Numerical Frequency (Hz)	Experimental Frequency (Hz)
(1,0,0)	88.9	88
(0,0,1)	111.4	111
(0,1,0)	140.6	139
(1,0,1)	142.5	142
(1,1,0)	166.3	170
(2,0,0)	177.7	182.5
(0,1,1)	179.3	182.5
(1,1,1)	200.1	199
(2,0,1)	209.7	207.5

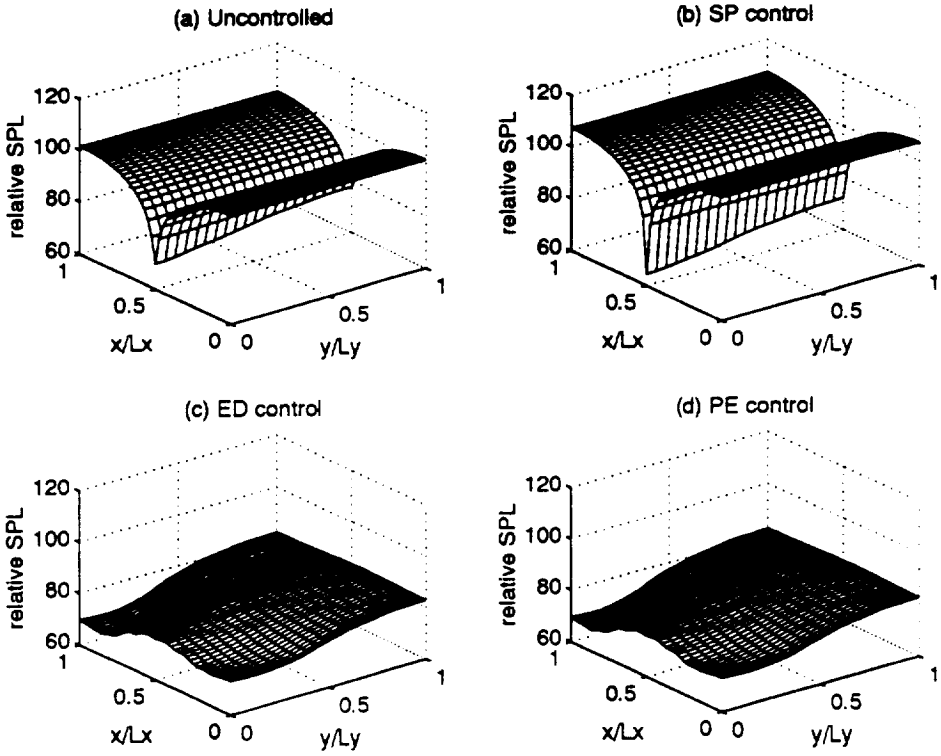

Figure 20. Predicted sound pressure distribution for the plane z = 0.76 m. (88.9 Hz - (1,0,0) mode).

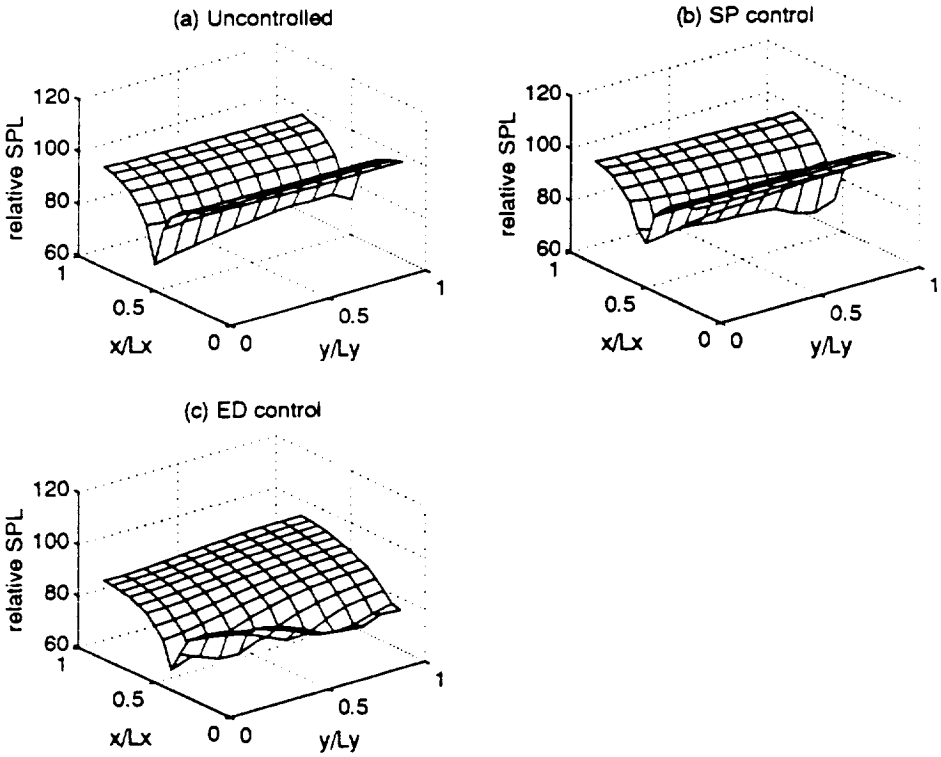

Figure 21. Experimental sound pressure distribution for the plane z = 0.76 m. (88 Hz - (1,0,0) mode).

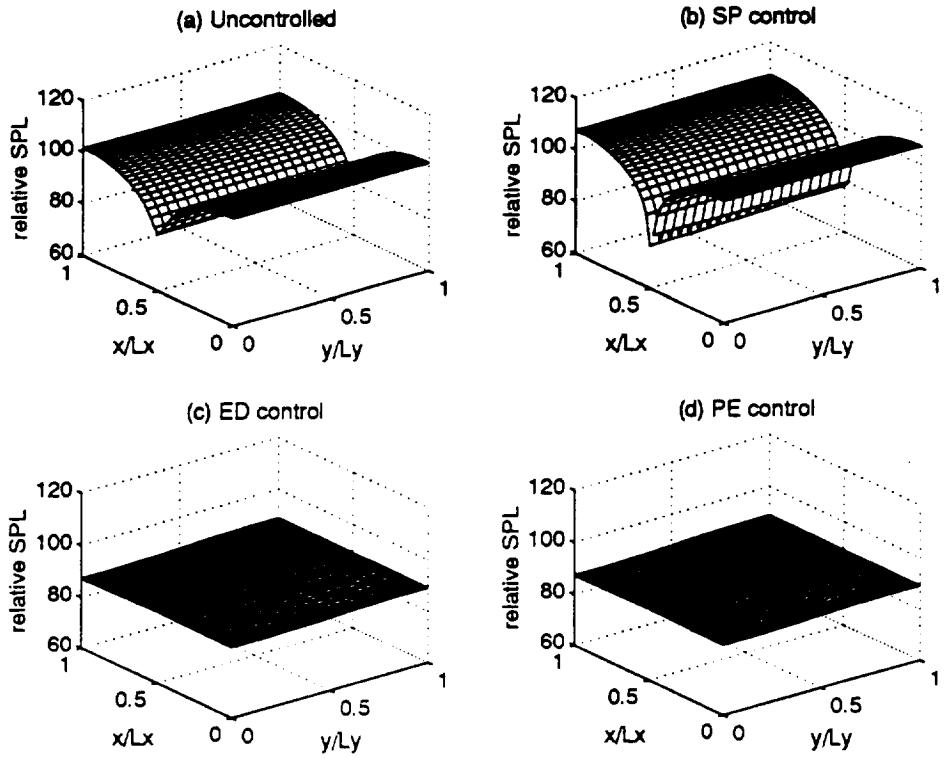

Figure 22. Predicted sound pressure distribution for the plane z = 1.28 m. (88.9 Hz - (1,0,0) mode).

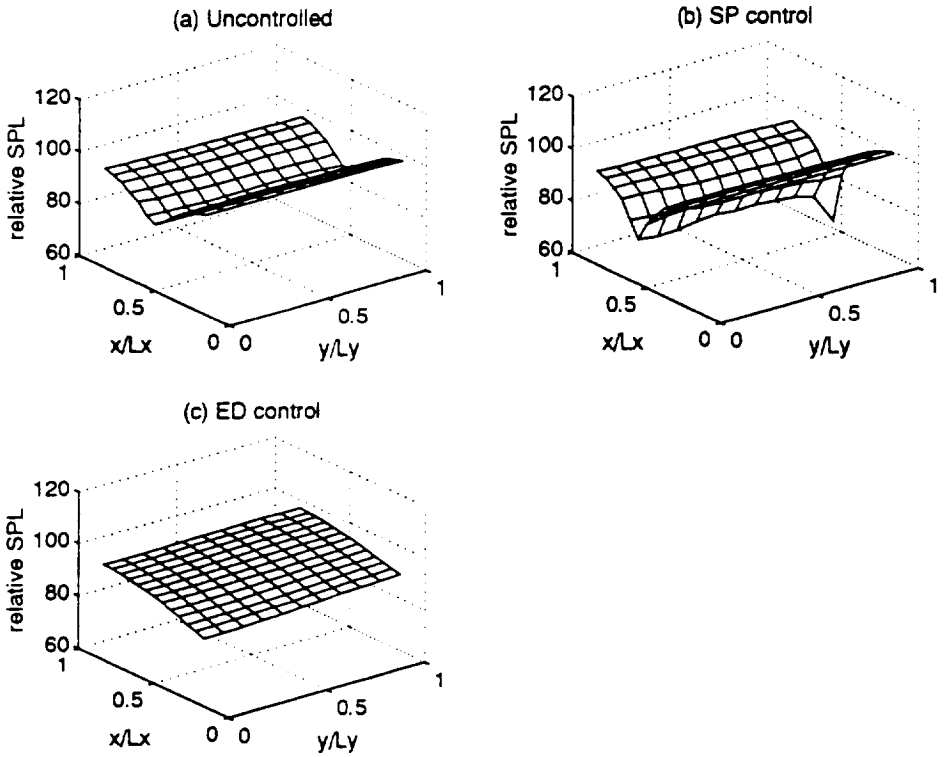

Figure 23. Experimental sound pressure distribution for the plane z = 1.28 m. (88 Hz - (1,0,0) mode).

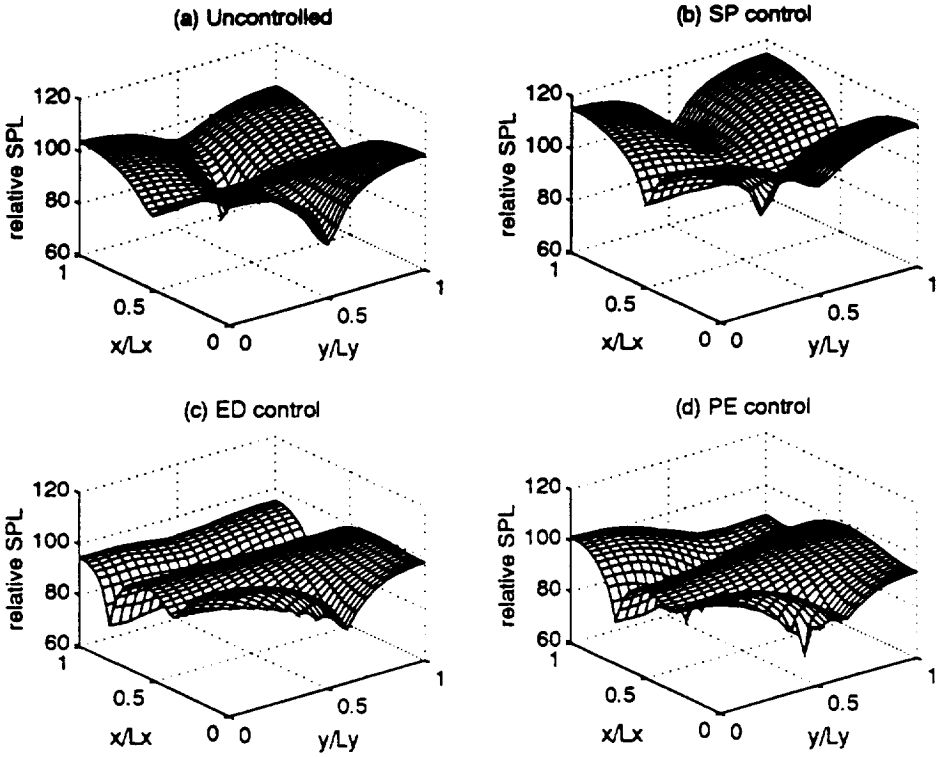

Figure 24. Predicted sound pressure distribution for the plane z = 0.25 m. (166.3 Hz - (1,1,0) mode).

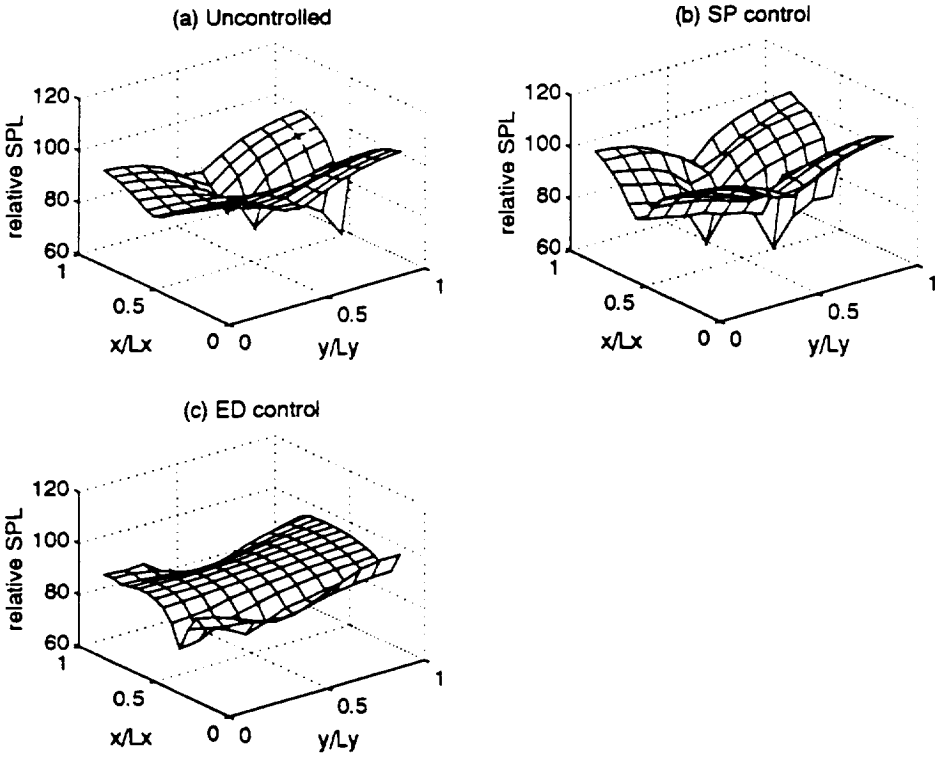

Figure 25. Experimental sound pressure distribution for the plane z = 0.25 m. (170 Hz - (1,1,0) mode).

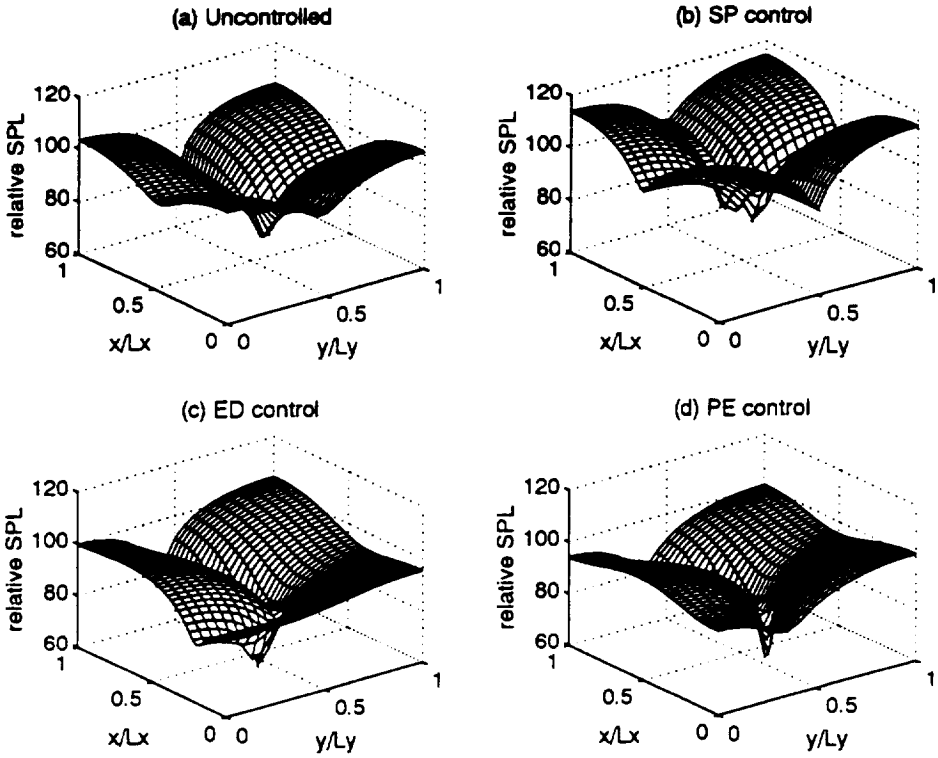

Figure 26. Predicted sound pressure distribution for the plane z = 1.28 m. (166.3 Hz - (1,1,0) mode).

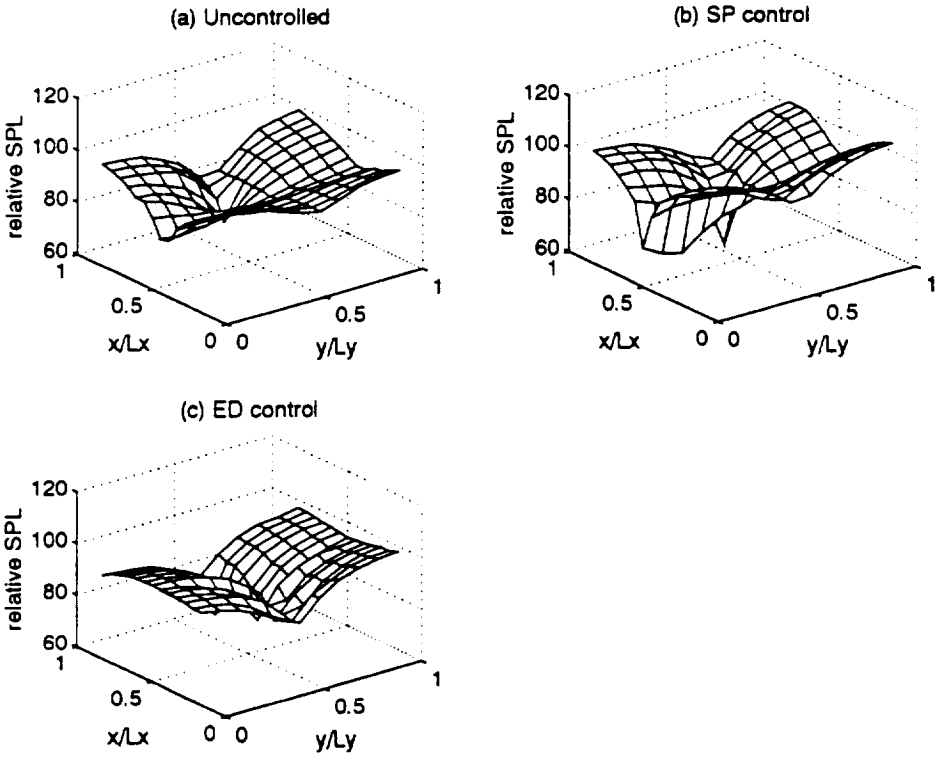

Figure 27. Experimental sound pressure distribution for the plane z = 1.28 m. (170 Hz - (1,1,0) mode).

to observe the dominant mode when minimizing the squared pressure, and local attenuation at the error sensor results with the level of the dominant (1,1,0) mode increasing throughout the enclosure. On the other hand, when the energy density is minimized, the error sensor is able to sense the dominant mode and attenuate its amplitude throughout the enclosure. It can be seen from Figures 24 and 25 for the $z = 0.25$ m plane that the residual acoustic field closely resembles the (2,0,0) mode, which can be seen from Table 1 to be the residual mode whose resonance frequency is closest to the excitation frequency of 170 Hz. It can again be seen that there is reasonable agreement between the spatial dependence obtained experimentally and the spatial dependence predicted numerically.

The global potential energy in the enclosure can be determined by integrating the squared pressure over the volume of the enclosure[5]. For the case of the experimental results, this was approximated by summing up the squared pressures from the measurement grid points, in this case given as

$$E_p(dB) = 10\log_{10}\left(\sum_{ix=1}^{13}\sum_{iy=1}^{11}\sum_{iz=1}^{5} p^2(ix,iy,iz)\,dx\,dy\,dz\right), \qquad (11)$$

where $dx = 0.1$ m, $dy = 0.11$ m, and $dz = 0.25$ m. The results are shown in Table 2 for the (1,0,0) and (1,1,0) modes, and the attenuation of the potential energy achieved is shown in Figure 28. For the numerical results, the attenuation in the potential energy is shown for minimizing the squared pressure, the energy density, and the potential energy. For the experimental results, the attenuation is shown for controlling the squared pressure and the energy density. It can be seen that the predicted trends are observed experimentally in both cases. The attenuation achieved when controlling energy density and the amplification achieved when controlling the squared pressure is not as large as predicted. It is thought that this may in part be due to the missing grid points along the x-axis, due to the nature of the traversing mechanism. The largest reductions would be expected to occur near the walls of the enclosure, so that these missing points could lead to the results

Table 2. Potential Energy (dB) in the Enclosure With and Without Control.

	Uncontrolled	Squared Press. Control	Energy Density Control	Potential Energy Control
Numerical:				
(1,0,0) mode (88.9 Hz)	12.6	18.4	0.3	0.3
(1,1,0) mode (166.3 Hz)	12.3	22.6	9.6	8.4
Experimental:				
(1,0,0) mode (88 Hz)	3.1	3.9	-0.1	
(1,1,0) mode (170 Hz)	2.7	7.0	1.4	

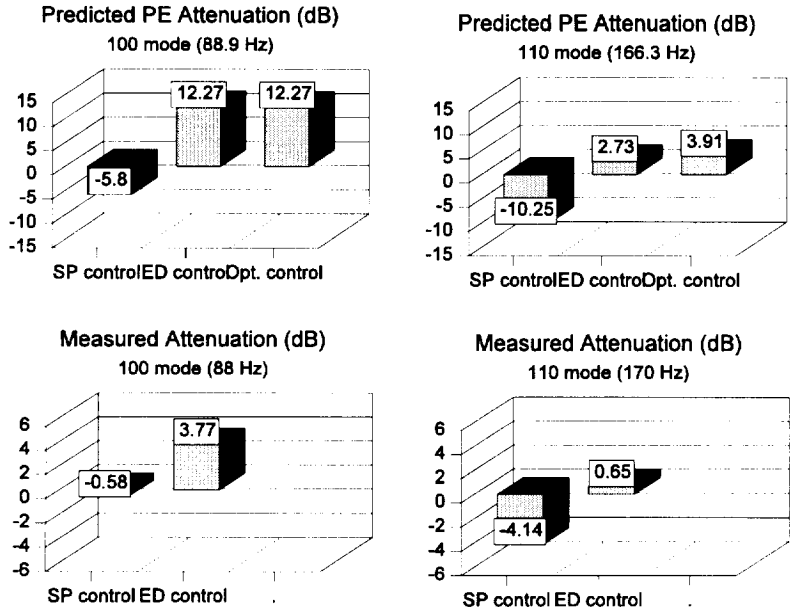

Figure 28. Predicted and measured attenuations of the global potential energy.

observed. Nonetheless, the results do demonstrate that for these cases the minimization of energy density leads to significantly improved global control of the acoustic field.

4.3.4. Results Using Multiple Sources and/or Sensors

Experimental results were also obtained for a number of multiple source and/or sensor configuration, for comparison with numerical predictions. For the experimental results, both the squared pressure and the energy density were used as acoustic variables to be minimized. Figures 29-32 show one example of typical results obtained for multiple source/sensor configurations. For these results, the primary source is at a normalized location of (0.01,0.01,0.99) and excites the field at a frequency of 89 Hz. There are two control sources, located at (0.99,0.01,0.99) and (0.99,0.623,0.026), and two error sensors (either pressure or energy density), located at (0.41,0.17,0.61) and (0.18,0.73,0.25). For both control methods, the predicted and measured pressure fields were obtained for various horizontal planes in the enclosure. Figures 29 and 30 show the predicted and measured results for the $z = 0.43$ m plane, while Figures 31 and 32 show the same results for the $z = 0.67$ m plane. It can be seen that the agreement between the numerical and measured results is quite good. In addition, the method of minimizing the energy density more closely approximates the field that one would obtain if the global potential energy is minimized.

Table 3 shows the global results obtained for the frequency of 89 Hz. Two different configurations are represented in this table: one with a single control source, and one with two control sources. Again there is reasonable agreement between the numerical and experimental results.

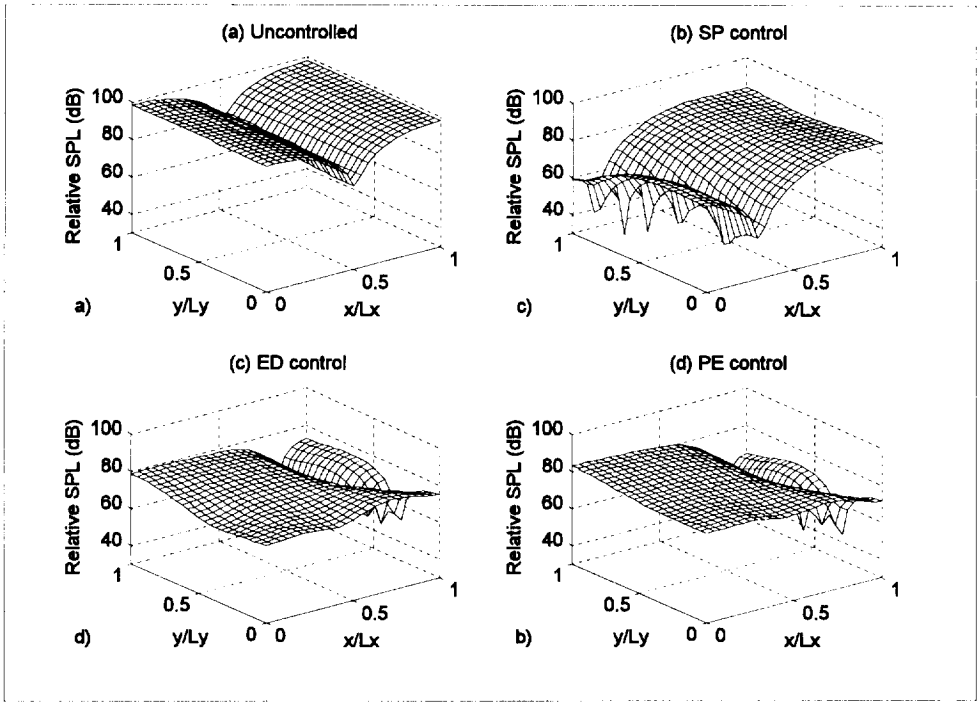

Figure 29. Predicted sound pressure distribution: z = 0.43 m, 88.9 Hz, (1,0,0) mode, 2 error sensors, 2 control sources.

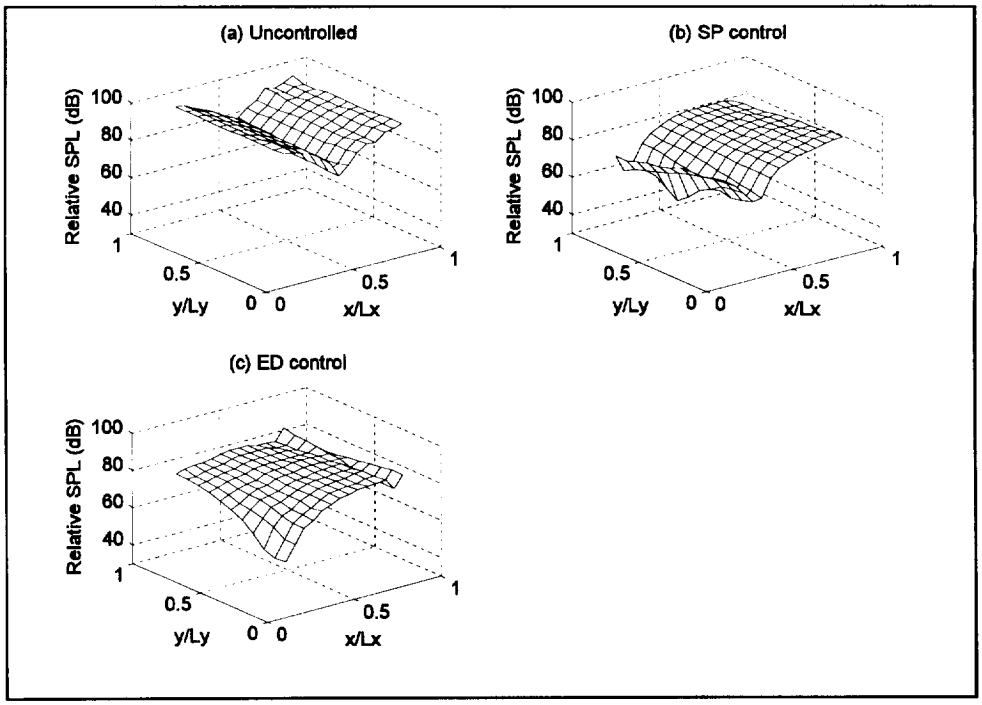

Figure 30. Experimental sound pressure distribution: z = 0.43 m, 90 Hz, (1,0,0) mode, 2 error sensors, 2 control sources.

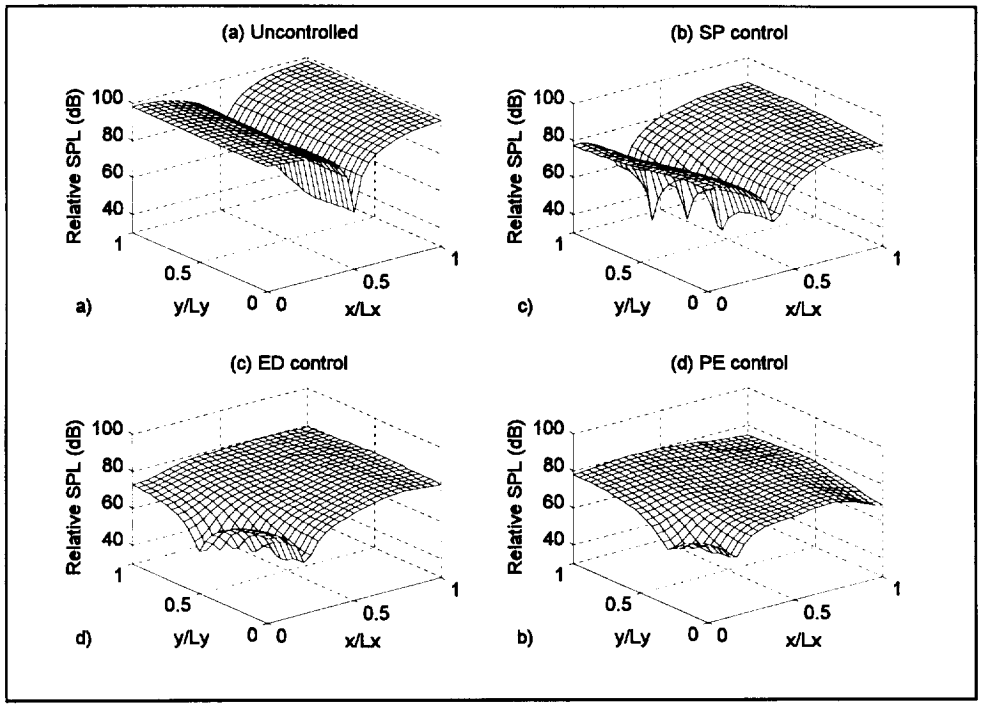

Figure 31. Predicted sound pressure distribution: z = 0.67 m, 88.9 Hz, (1,0,0) mode, 2 error sensors, 2 control sources.

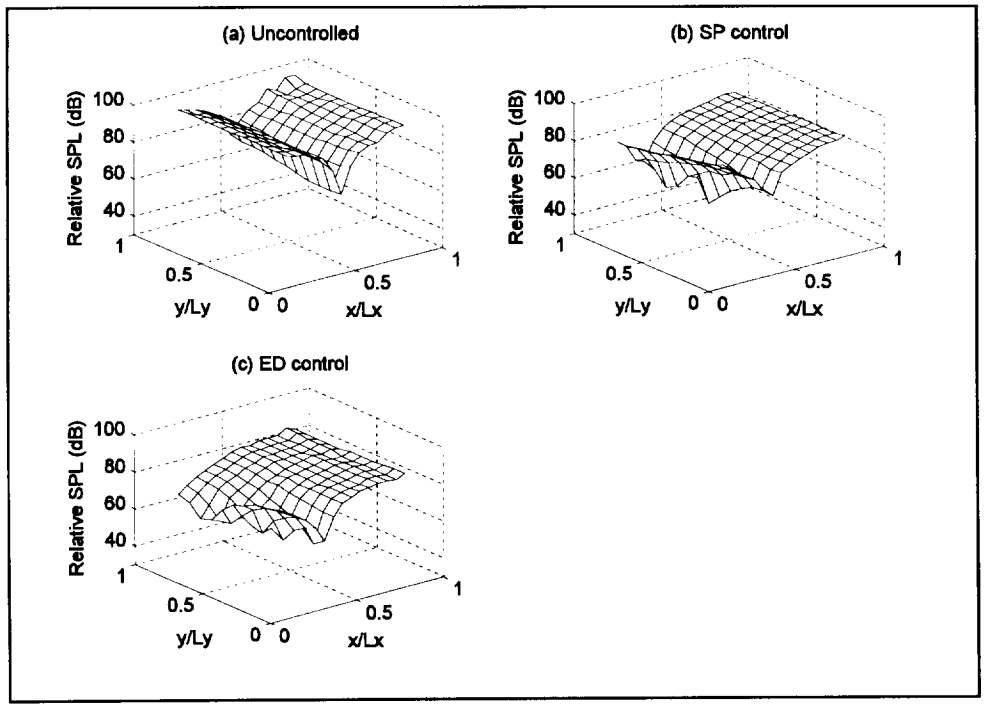

Figure 32. Experimental sound pressure distribution: z = 0.67 m, 90 Hz, (1,0,0) mode, 2 error sensors, 2 control sources.

Table 3. Global Potential Energy in the Enclosure (89 Hz).

	Uncontrolled	Squared Press. Control	Energy Density Control	Potential Energy Control
Numerical:				
2 sensors, 1 source	95.0	86.6	85.0	84.0
2 sensors, 2 sources	95.0	83.2	81.4	79.6
Experimental:				
2 sensors, 1 source	94.5	87.9	85.1	
2 sensors, 2 sources	94.5	86.2	83.5	

5. Conclusions and Recommendations For Future Energy Density Control Research

Previous research on one-dimensional fields had indicated that significantly improved global attenuation could be obtained by minimizing the acoustic energy density, rather than the squared pressure. The research reported here has extended this prior research to three-dimensional fields. Many of the same conclusions reached earlier are still applicable, but there are some complicating factors that have arisen.

For a one-dimensional field, the energy density is constant throughout the field, and as a result, there is not dependence on error sensor location when minimizing the energy density. For a three-dimensional field, the energy density is not constant, and as a result, there is some dependence on sensor location. However, the nodal surfaces associated with the energy density represent a significantly smaller fraction of the enclosure volume, so that the method of minimizing energy density is still significantly less sensitive to sensor location that for minimizing squared pressure. This is an attractive feature of the approach for practical implementations, where it often may not be possible to locate the error sensors in the optimal locations.

To actively minimize the energy density in the enclosure requires a sensor that allows one to measure both the pressure and the particle velocity. This requires multiple transducers. One of the results of this research is that a low-cost sensor has been developed that provides the information necessary to implement the active control of energy density. The relatively low cost of the "energy density sensor" makes the implementation of the approach practical for a number of applications, including the active control of interior aircraft fields.

The active control of energy density has been examined both numerically and experimentally in this research. It has been found that one can typically achieve global attenuation of the field when controlling energy density that is at least as great as when controlling the squared pressure, and is often greater. If one compares the results in terms of sensor sites, one can nearly always achieve improved control using energy density with N sensors over using squared pressure with N sensors. On the other hand, if one compares the results in terms of total number of transducers used, the control achieved is generally comparable between the two methods when N transducers are used. There are still several advantages to using energy density, however. The method of minimizing energy density is much less sensitive to error sensor location. In addition, the possibility exists to achieve greater simplification of the control system when minimizing the energy density.

This research has also pointed out a number of areas where additional research would be very beneficial. Some of these additional research areas include the following:

i) The current "energy density sensor" used provides six pressure signals to the DSP board, and the quantities required for control implementation are computed internally in software. However, it became apparent that in addition to using energy density for control, significant insights into acoustic fields could be obtained by looking at the energy density field, as opposed to the pressure field. In this context, it would be very useful to modify the "energy density sensor" so that the circuitry of the sensor itself resulted in an output proportional to

the measured energy density. This would allow one to use the sensor to map acoustic fields in terms of energy density.

ii) In many applications, there is some knowledge of the acoustic field that would make it possible to modify the energy density sensor design to take advantage of that knowledge. In this manner, it may be possible to simplify the sensor and perhaps reduce the total number of transducers, without sacrificing the benefits of minimizing the energy density. For example, if the sensor were placed near a hard surface, one could make the assumption that the normal velocity component is very small, thereby reducing the number of velocity components required by one.

iii) One of the findings of this research is that one often does not achieve significant increases in the global attenuation by adding additional energy density sensors beyond a certain relatively small number. However, the control achieved also depends on the number of control sources used, and one may typically achieve improved control by adding additional actuators. Currently, the control system requires at least as many sensors as actuators for proper operation. Thus, one objective of future research would by to modify the control system to allow the user to have more control sources than error sensors. This will involve the implementation of a constrained optimization procedure to overcome the overdetermined nature of the control problem.

iv) The focus of this research project was on actively controlling acoustic fields at low frequencies where one can assume a relatively low modal density. It would also be useful to investigate the effectiveness of minimizing energy density for the high modal density case. Preliminary analysis has indicated that one would achieve a local control effect, but it is not certain how the extent of this control would compare to the control obtained when minimizing the squared pressure under these conditions.

6. References

1. P. A. Nelson, A. R. D. Curtis, S. J. Elliott, and A. J. Bullmore, "The active minimisation of harmonic sound fields, Part I: Theory," *J. Sound Vib.*, **117**, 1-13 (1987).

2. Nashif, P. J. "An energy-density-based control strategy for minimizing the sound field in enclosures," M.S. thesis, The Pennsylvania State University, University Park, PA (1992).

3. Sommerfeldt, S. D. and Nashif, P. J., "An adaptive filtered-*x* algorithm for energy-based active control," *J. Acoust. Soc. Am.*, **96**, 300-306 (1994).

4. S. D. Sommerfeldt and J. W. Parkins, "An evaluation of active noise attenuation in rectangular enclosures," *Proc. Inter-Noise 94*, 1351-1356 (1994).

5. S. D. Sommerfeldt, J. W. Parkins and Y. C. Park, "Global active noise control in rectangular enclosures," *Proc. Active 95*, Newport Beach, CA, July 6-8, 1995, pp. 477-488.

6. G. W. Elko, "An acoustic vector-field probe with calculable obstacle bias," *Proc. Noise-Con 91*, 525-532 (1991).

7. T. Hodges, P. A. Nelson, and S. J. Elliott, "The design of a precision digital integrator for use in an active vibration control system," *Mech. Systems Sig. Proc.*, **4**, 345-353 (1990).

8. B. Widrow and S. D. Stearns, *Adaptive Signal Processing* (Prentice-Hall, Inc., Englewood Cliffs, N. J.) 1985.

9. S. D. Sommerfeldt, "Multi-channel adaptive control of structural vibration," *Noise Control Eng. J.*, **37**, 77-89 (1991).